Theoretical And Experimental Analyses
Of
All-Optical Gain-Clamped L-Band EDFAs

Bing Xia

Photonic Systems Group
Electrical & Computer Engineering
McGill University
Montreal, Canada
June, 2002

This thesis is submitted to the Faculty of Graduate Studies and Research in partial fulfillment of the requirements of the degree of Master of Engineering

National Library
of Canada

Acquisitions and
Bibliographic Services

395 Wellington Street
Ottawa ON K1A 0N4
Canada

Bibliothèque nationale
du Canada

Acquisisitons et
services bibliographiques

395, rue Wellington
Ottawa ON K1A 0N4
Canada

Your file Votre référence
ISBN: 0-612-85901-0
Our file Notre référence
ISBN: 0-612-85901-0

Abstract

A systematic analysis of all-optical gain-clamped L-band EDFAs for long-haul DWDM transmission systems is presented in this thesis. A full numerical model is used to simulate and fully characterize the performance and properties of single-stage and two-stage EDFAs. We focus on two configurations of two-stage L-band EDFAs with gain-clamped characteristics using partial gain-clamping. Partial gain-clamping is obtained by forming a fiber grating laser in either the first or the second stage of the two-stage EDFA.

From our simulation and experimental results, we conclude the following: (1) a good gain-clamping effect can be achieved by partially gain-clamped configurations in which only one stage (first or second) is truly clamped; (2) an inherent low noise figure can also be obtained when the second stage is clamped; (3) the selection of feedback wavelengths and feedback levels are critical for obtaining a flat gain spectrum and low noise performance; (4) small transient gain (power) excursions can be realized with partially clamped configurations and relaxation oscillations are well suppressed when a high feedback level is used without large degradation in either the gain or noise figure.

Résumé

Dans cette thèse, nous présentons une analyse systématique des amplificateurs optiques à fibres dopées à l'erbium (EDFA) avec saturation de gain, opérationnels dans la bande L, pour les systèmes de canaux de multiplexage dense en longueur d'onde (DWDM). Un modèle numérique complet est utilisé pour effectuer les simulations et déterminer les charactéristiques ainsi que les propriétés des amplificateurs à un ou deux étages. En particulier, notre analyse porte sur deux configurations de EDFA à deux étages, en saturation partielle, ayant les caractérisiques de saturation de gain. L'opération en saturation partielle est obtenue en formant un laser de fibre optique avec des filtres de Bragg dans l'un des deux étages de l'amplificateur.

Nos simulations, ainsi que nos résultats expérimentaux nous permettent de conclure ce qui suit:

1) Une bonne opération en saturation de gain peut être obtenue par saturation partielle de l'amplificateur, où juste un seul des deux étages est saturé.
2) De plus, une basse figure de bruit peut etre obtenue lorsque le deuxième étage fonctionne en saturation de gain.
3) Le choix des longeurs d'onde ainsi que du niveau de rétroaction optique est primordial afin d'obtenir un spectre de gain plat et un bas niveau de bruit.
4) L'opération en saturation de gain partielle permet de réduire des fluctuations dynamiques de gain, et un niveau de retroaction optique élevé supprime majoritairement les oscillation de relaxation.

Acknowledgements

I would like to thank to my supervisor ***Prof. Lawrence R. Chen*** for his superb guidance, support and constant encouragement throughout my thesis writing and the whole research work. I deeply appreciated his instructive teaching from theoretical model to experiments and beyond.

I would like to thank all members in Photonic System Group at *McGill University* for their support in the last two years. Special thanks to ***Shiwei Huang*** for his helpful discussion on numerical models in my simulation and ***Dominik Pudo*** for his great help on making tunable fiber Bragg gratings, one of the most important components used in my experiments.

I would also like to thank ***Peter Chan*** and Bragg Photonics Inc. for providing various components used in my experiments.

This research was supported by the Canadian Institute for Telecommunications Research, the Natural Sciences and Engineering Research Council (Canada), and the McGill University Faculty of Graduate Studies and Research.

Contents

List of Figures

List of Tables

Chapter 1. Introduction and Motivation

1.1 Introduction to EDFA

Erbium-doped fiber amplifiers (EDFAs) are one of the key components for current optical transmission networks and their applications have transformed the optical communications industry.

The first erbium-doped single-mode fiber amplifiers for signals at $1.5\mu m$ were reported in 1987 simultaneously at the University of Southampton and AT&T Bell Laboratories [1.1,1.2]. The key achievement in their experiments was the recognition that erbium ions are ideally suited for optical amplification in modern optical fiber transmission systems operating at $1.5\mu m$. Since then, there has been considerable research exploring the fundamental properties and possible applications of EDFAs in optical networks [1.3-1.5]. EDFAs can be used as power amplifiers to boost the transmitter power, as in-line amplifiers to increase system reach, or as preamplifiers to enhance receiver sensitivity, all of which are indispensable components for realizing long-haul transmission.

There are plenty of advantages of using EDFAs as optical amplifiers in optical fiber networks. Before the advent of EDFAs, optoelectronic regenerators that include both a receiver and a transmitter were required to compensate attenuation in the middle of a transmission system. With EDFAs, lightwave signals are amplified purely in the optical domain: optical signals are amplified directly in optical format without the need for O/E/O conversion, thereby greatly reducing the complexity and cost of systems. Second,

EDFAs can be applied to both CW (continuous wave) signals and modulated signals if the modulation speed is greater than 1Mbit/s due to the long lifetime of erbium ions in the upper state. The most far-reaching impact is that EDFAs can be used to amplify many channels simultaneously, provided the channels lie within the bandwidth of the amplifier. This feature greatly pushes forward the development of dense wavelength division multiplexing (DWDM) systems.

1.2 Motivation for L-band Amplifiers and Gain-Clamping

In the last few years, DWDM systems have been widely deployed to increase the transmission capacity on single fibers in optical networks. DWDM is an optical transmission technology that couples many wavelengths in the same fiber, effectively increasing the aggregate bandwidth per fiber to the sum of the bit rates of each wavelength. However, the total bandwidth is not unlimited and aggregate system capacity is confined by the bandwidth of the optical amplifiers available in the market. Currently, the most popular optical amplifiers are C-band EDFAs (conventional band, with an operating wavelength range of 1530-1565nm) in which around 40 channels with a spacing of 100GHz can be placed. Although a large transmission capacity in the C-band can be achieved with leading-edge technology (i.e. narrower channel spacing), more transmission bandwidth with low operation cost is still urgently needed due to the fast increased requirements for new traffic such as IP and video services. On the other hand, optical fiber shows extremely low attenuation in the third communication window that is defined from 1450-1650nm, in which the C-band only covers a small fraction. Therefore,

it is necessary to study DWDM transmission in alternate wavelength bands, such as the long wavelength band (L-band, with an operating wavelength range of 1570nm-1610nm). As one of the key component for L-band transmission, research in L-band optical amplifiers has recently attracted a lot of attention.

It has been shown that EDFAs can also be designed to provide amplification in the L-band as well as in the C-band [1.6-1.8] using sufficiently long lengths of EDF. Hence, a DWDM system can operate in this band and double its total transmission capacity. Furthermore, gain control, which is a serious problem for C-band EDFAs, should also be taken into consideration carefully in L-band EDFAs for DWDM systems. This is because the total input signal power in a DWDM system to an EDFA can vary significantly as a result of channel add/drop operations or channel redistributions, possibly causing the degradation of system performance if no proper mechanisms are used to control the gain.

1.3 Current Technologies for Gain Control

1.3.1 Traditional Methods

There are two traditional approaches to do gain control: pump control and signal control [1.9]. Fig. 1.1 shows the typical configurations of these two methods based on ring feedback structures. In the method of pump control, a small portion of the output power is tapped, the probe signal is filtered out, detected, and used to define an electrical signal to the pump driver. When the input signal power varies, changes in the power of the probe signal can be detected at the feedback loop first; and then the pump driver circuit

will continuously adjust the pump power injected to the EDFA until the preset gain value of the probe signal is obtained. Meanwhile, there are also implementations that use an input tap to monitor the input signal power changes directly [1.9]. The purposes of these pump control methods are to suppress gain saturation by increasing or decreasing the pump power as the input signal power changes.

The signal control method as shown in Fig. 1.1(b) uses a similar feedback loop structure to monitor the variations of the signal power at the output. Instead of changing the pump power, an additional laser signal (auxiliary signal) is added at input and the power level injected to the amplifier can be adjusted based on its output power. The function of this additional signal is to compensate the variations of input signal power by keeping the total input power to the EDFA constant. Therefore, gain saturation of this amplifier is fixed to a level which leads to a clamped gain for all the input signals.

Although both methods are very effective in clamping the signal gain, there are also quite a few drawbacks. First, both require additional optical and optoelectronic

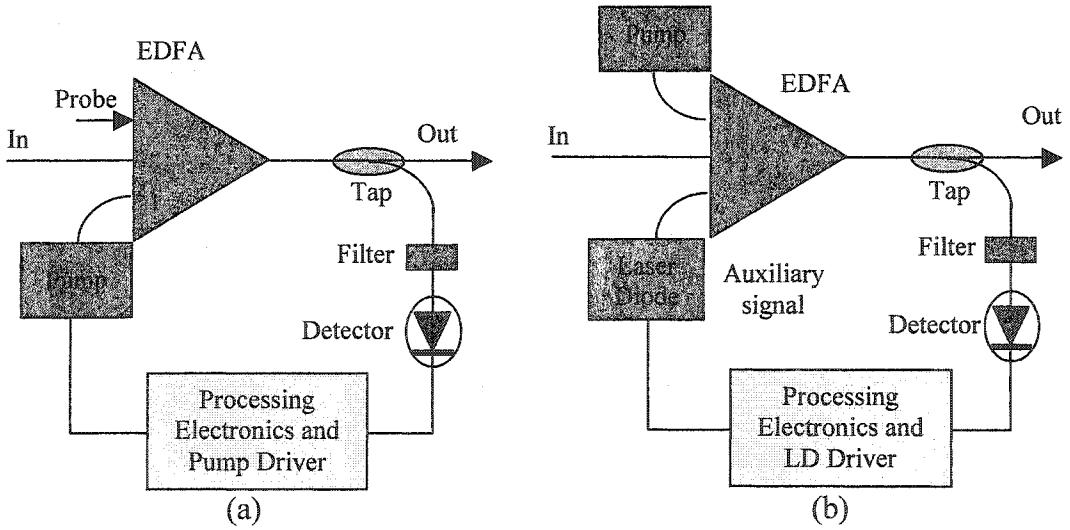

Fig. 1.1 Two traditional configurations for automatic gain control with a feedback loop structure (a) feedback with pump control (b) feedback with auxiliary signal control

devices such as a tap, filter and detector to pick up the optical probe signal, then process and generate an electronic control signal in the feedback loop in order to do gain control, thereby greatly increasing the cost. Second, gain-clamping is not self-regulated by the amplifier; i.e. it is controlled by processing electronics in addition to a pump driver circuit or LD driver circuit in the feedback loop. Therefore, the pump power or LD output power needs to be varied over a large range to compensate the gain variations; this requires a very complicated pump/LD driver circuit in order to achieve a better clamping performance.

1.3.2 All-Optical Gain Control with Ring Laser Structure

An alternate method for gain control involves the use of a feedback ring laser [1.10,1.11]. The typical configuration (denoted as a ring laser configuration) is shown in Fig. 1.2, in which the feedback loop only consists of a few passive, all-optical devices. In this method, gain control is done purely in the optical domain without any optical-to-electrical conversion.

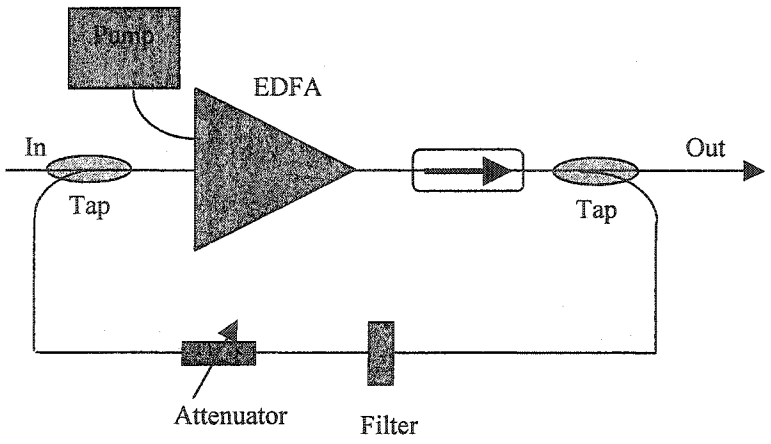

Fig. 1.2 Configuration of gain-clamped EDFAs with a feedback ring loop

The theory of gain clamping in this configuration is similar to the 'signal control' method described in section 1.3.1. However, the auxiliary signal is not generated by a separate laser diode, but rather an erbium-doped fiber ring laser (EDFRL) that is incorporated into the amplifier. This lasing signal comes into the amplifier together with the data (DWDM) signals. Note that the lasing signal can co-propagate or counter-propagate with the input signals. Due to the lasing condition (i.e. in steady state, the gain should be equal to the total cavity loss), the gain of this lasing signal inside the amplifier is clamped to a level which in turn fixes the average inversion level N_2 of the EDFA (the details can be seen in Chapter 2). Fig. 1.3 shows the gain coefficient spectra for different value of the average inversion level N_2. It can be seen that a given inversion level corresponds to one gain level for each wavelength and vice versa. Hence, a fixed gain level at the lasing wavelength fixes the whole gain spectrum. We will discuss the inversion level and clamping theory in later sections.

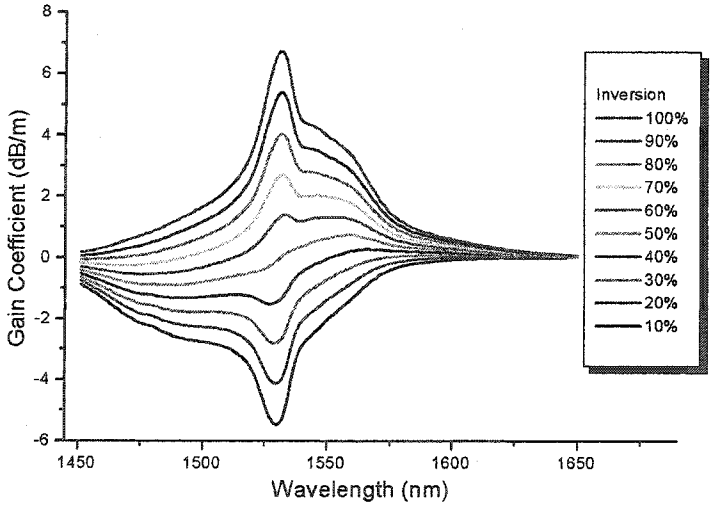

Fig. 1.3 Gain coefficient spectrums at different average inversion levels

1.3.3 All-Optical Gain Control with Fiber Bragg Gratings

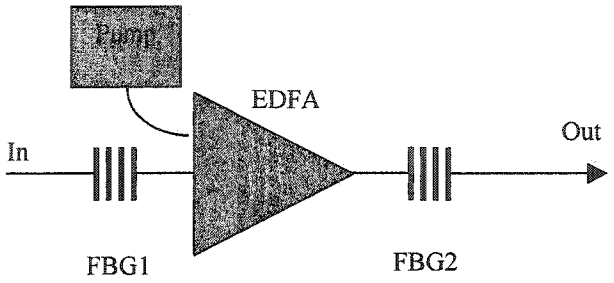

Fig. 1.4 Configuration of gain-clamped EDFA with FBG fiber laser structure

After the invention of ring laser structures for gain control, a simpler design has been demonstrated to have good gain-clamping effect (denoted as FBG configuration) [1.12,1.13]. As shown in Fig. 1.4, a pair of fiber Bragg gratings (FBGs) is placed on both ends of a conventional amplifier. An FBG is a periodic perturbation of the refractive index along the fiber length which is formed by exposure of the core of the optical fiber to an intense optical interference pattern [1.14,1.15]. The main function of the FBG is to reflect an incoming optical signal at the Bragg wavelength. Therefore, if we choose FBG1 and FBG2 in Fig. 1.4 with the same Bragg wavelength, an erbium-doped fiber grating laser (EDFGL) is formed. The lasing signal in this configuration has exactly the same function as in the ring laser configuration described in section 1.3.2, which can effectively clamp the signal gains. The advantages of this structure are obvious: (1) it saves a lot optical devices such as a tap, optical filter and optical attenuator; (2) the fiber grating can be made directly in the erbium-doped fiber, which avoids additional losses associated with fiber splicing; and (3) very low cavity loss can be realized by using FBGs with high reflectivities. In the ring laser configuration, a tap is used at output to switch a

small portion of optical power to the feedback loop. This portion must be very small in order to minimize the loss of the signal power and therefore, the total cavity loss is generally quite large. For the FBG configuration, the cavity loss can range from 1dB to 20dB by choosing FBGs with proper reflectivities, which gives more flexibility to the EDFA design. Furthermore, the FBGs can be very narrowband and the feedback level can be chosen very high without creating loss for the signal wavelength.

1.4 Thesis Outline

This thesis includes systematic studies of all-optical gain-clamped L-band EDFAs and is based on two papers: (1) "*Two-stage L-band EDFA with gain-clamped characteristics using partial gain-clamping*" [1.16] and (2) "*Comparison of Two-Stage L-band EDFAs with Gain-Clamped Characteristics Based on Three Configurations*" [1.17]. In this thesis, more in-depth details and discussions are presented, especially on the simulation models and dynamic performance.

The remainder of this thesis is organized as follows. In Chapter 2, we will first introduce some basic properties of erbium-doped fiber. Then, we describe the models that are commonly used to simulate the behavior of EDFAs. The gain-clamped model we used in our simulations is also presented in detail.

In Chapter 3, we investigate the static properties of single-stage gain-clamped L-band EDFAs with ring laser configurations and FBG configurations using numerical simulations. We systematically study and evaluate the clamping effect and gain/NF spectra for both configurations with different feedback conditions.

In Chapter 4, two configurations of two-stage L-band EDFAs with gain-clamped characteristics using partial gain-clamping are proposed and analyzed. Both configurations, in which only one stage is truly clamped, have been modeled and experimentally characterized. We measure the gain dynamics and analyze the dynamic properties in Chapter 5. In Chapter 6, we summarize our results and discuss future work of gain-clamped L-band EDFAs.

References

[1.1] R.J. Mears, L. Reekie, I.M. Jauncey, and D.N. Payne, " Low-noise erbium-doped fiber amplifier operating at 1.54μm ," *Electron. Lett.*, vol. 23, no. 19, 1987.

[1.2] E. Desurvire, J.R. Simpson and P.C. Becker, "High-gain erbium-doped traveling wave fiber amplifier," *Optics Letter*, vol. 12, no.11, 1987.

[1.3] D. Will and B. Teichmann, "Design of erbium-doped fiber amplifiers for telecommunication systems," *Electronic Components and Technology Conference*, Proceedings, 44th, pp. 293-297, 1994.

[1.4] TingYe Li, "The Impact of Optical Amplifiers on Long-Distance Lightwave Telecommunications," *Proceedings of the IEEE*, vol. 81, no. 11, pp. 1568 –1579, 1993.

[1.5] D.Bayart, B. Clesca, L. Hamon and J.L. Beylat, "1.55um fluoride-based EDFA with gain-flatness control for multiwavelength applications," *Electron. Lett.*, vol.30, no.17, pp. 1407-1409, 1994.

[1.6] Y. Sun, J. W. Sulhoff, A. K. Srivastava, J. L. Zyskind, T. A. Strasser, J. R. Pedrazzani, C. Wolf, J. Zhou, J. B. Judkins, R. P Espinolda, and A. M. Vengsarkar, "80 nm ultra-wideband erbium-doped silica fiber amplifier," *Electron. Lett.*, vol. 33, no. 23, pp. 1965-1967, 1997.

[1.7] T.-C. Liang, Y.-K. Chen, J.-H. Su, W.-H. Tzeng, C. Hu, Y.-T. Lin, Y.-C. Lai, "Optimum configuration and design of 1480-nm pumped L-band gain-flattened EDFA using conventional erbium-doped fiber," *Opt. Commun.*, vol. 183, nos. 1-4, pp. 51-63, 2000.

[1.8] M. Karásek, "The design of L-band EDFA for multiwavelength applications," *J. Opt. A: Pure Appl. Opt.*, vol. 3, pp. 96-102, 2001.

[1.9] E. Desurvire, "Erbium-Doped Fiber Amplifiers-Principles and Applications," *John Wiley & Sons, Inc.* 1994.

[1.10] M. Zirngibl, "Gain control in erbium-doped fiber amplifiers by an all-optical feedback loop," *Electron. Lett.*, vol. 27, no. 7, pp. 560-561, 1991.

[1.11] A. Yu and M.J. O'Mahony, "Properties of gain controlled erbium doped fiber amplifiers by lasing," *Electron. Lett.*, vol. 31, no. 16, pp.1348-1349, 1995.

[1.12] E. Delevaque, T. Georges, J.F. Bayon, M. Monerie, P.Niay and P.Bernage, "Gain control in erbium-doped fiber amplifiers by lasing at 1480nm with photoinduced Bragg gratings written on fiber ends," *Electron. Lett.*, vol. 29, no.12, pp. 1112-1114, 1993.

[1.13] Y. Zhao, J. Bryce, and R. Minasian, "Gain clamped erbium-doped fiber amplifiers—Modeling and experiment," *IEEE J. Sel. Topics in Quantum Electron.*, vol. 3, no. 4, pp. 1008-1012, 1997.

[1.14] K. O. Hill, Y. Fujii, D.C. Johnson, and B.S. Kawasaki, "Photosensitivity in optical fiber waveguides: Application to reflection filter fabrication," *Appl. Phys. Lett.*, vol. 32, pp. 647-649, 1978.

[1.15] K. O. Hill and G. Meltz, "Fiber Bragg Grating Technology Fundamentals and Overview," *IEEE J. Light. Tech.*, vol. 15, no. 8, pp. 1263-1276, 1997.

[1.16] B. Xia and L. R. Chen, "Two-stage L-band EDFA with gain-clamped characteristics using partial gain-clamping", *Opt. Commun.*, vol. 206, nos. 4-6, pp.301-308, 2002.

[1.17] B. Xia and L.R. Chen and P. Chan, "Comparison of Two-Stage L-band EDFAs with Gain-Clamped Characteristics Based on Three Configurations," *Optical Fiber Communications Conference 2002,* paper ThGG23.

Chapter 2 Modeling of EDFAs

2.1 Fundamental Properties of EDFAs

Before we present the models for EDFAs, we start by introducing some of fundamental properties of erbium-doped fiber (EDF).

2.1.1 Absorption and Emission Cross Sections

Absorption and emission cross sections are two of the most important parameters for EDFs. They quantify the ability of an erbium ion in the EDF to absorb and emit light. To be more accurate, the cross sections represent the probabilities of transitions to occur between ground state and excited state. For example, given two states 1 and 2, the probability that a photon is absorbed and emitted is proportional to the absorption cross section σ_{12}^{a} and emission cross section σ_{21}^{e}, respectively. Therefore, the total change in power of a light beam at a single wavelength of intensity I is given by:

$$\Delta P_{\lambda} = P_{\lambda}^{e} - P_{\lambda}^{a} = (N_2\sigma_{\lambda}^{e} - N_1\sigma_{\lambda}^{a})I \qquad (2.1)$$

This equation can be used to explain the amplification or attenuation of light propagating through the EDF. It notes that the emission and absorption probabilities are proportional to the light intensity rather than the light power. Since the light intensity is inversely proportional to the effective cross-sectional area (denoted as A_{eff}), A_{eff} is also important in determining the probabilities of absorption and emission.

2.1.2 The Overlap Factor and A_{eff}

In order to obtain the effective area of the absorption and emission cross sections, the transverse shape of the optical mode and its overlap with the transverse erbium ion distribution profile are very important since only the portion of the optical mode that overlaps with the erbium ion distribution will impact on absorption and emission. The overlap factor Γ is defined as a parameter to describe the relation between the optical mode and the erbium ion distribution. Generally, part of the optical mode will propagate in the cladding but erbium ions are typically doped in the core of the fiber. Therefore, the overlap factor is always less than 1.

The effective cross-sectional area is decided by the shape of the erbium ion distribution and can be obtained by $A_{eff} = \pi R^2$, where R is the equivalent flat top radius of the erbium ion distribution. Since the actual transverse distribution of erbium ions is

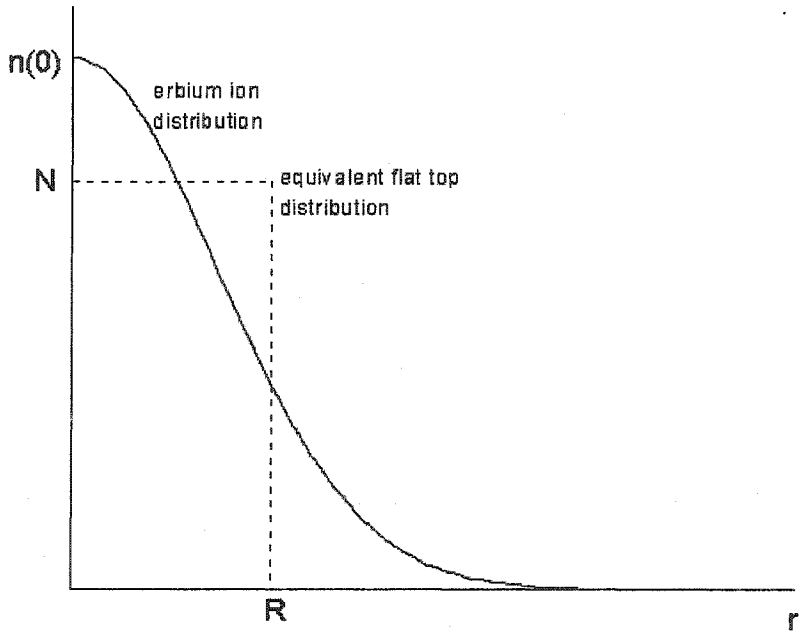

Fig. 2.1 The profile of erbium ion distribution and its equivalent flat top distribution.

hard to obtain, A_{eff} is usually used to simply the calculation in the model. Fig.2.1 shows an example of an equivalent flat top distribution and the actual erbium ion distribution. The radius R of the flat top distribution is determined by the geometric profile of the actual erbium ion distribution.

2.1.3 Amplified Spontaneous Emission

Spontaneous emission is an important phenomenon in optical amplifiers. The excited erbium ion can spontaneously relax to the ground state and emit a photon that is unrelated to the input signal wavelength. In an EDFA, photons at random wavelengths are generated and propagate in both forward and backward directions. These photons can be further amplified along the rest of the EDF as signals and therefore, they are referred to as ASE (amplified spontaneous emission). The ASE can saturate the pump power and limit the total amount of signal gain available from the amplifier. Furthermore, it decreases the optical signal-to-noise-ratio (OSNR), which is an important parameter in long-haul transmission systems.

The basic element of ASE power is the equivalent noise power, which is defined as the power generated in a point of EDF by spontaneous emission at frequency ν and in a bandwidth of $\Delta\nu$. Since there are two independent polarizations for a given frequency, the equivalent noise power can be expressed as:

$$P_{ASE}^{0} = 2h\nu\Delta\nu \tag{2.2}$$

Once generated, the equivalent noise power can be treated as a signal propagating in the amplifier. The whole ASE spectrum can then be divided into many small bandwidths

according to the resolution requirements and treated separately as many equivalent noise powers propagating in the amplifier. Further details can be found in the modeling section of this chapter.

2.1.4 Lifetime

The lifetime of an upper state is another important parameter in modeling EDFAs. It characterizes the average time that photons remain in the excited level before they decay to the ground state. For EDFAs, the lifetime is related to two main paths for decay: radiative and nonradiative transitions. Since the lifetime is inversely proportional to the probability of decay of the erbium ion, the total lifetime can be obtained by:

$$\frac{1}{\tau} = \frac{1}{\tau_r} + \frac{1}{\tau_{nr}} \tag{2.3}$$

where τ is the total lifetime, and τ_r and τ_{nr} are the radiative and non-radiative lifetimes, respectively. The radiative lifetime results from fluorescence from the excited level to all other levels below it, while the non-radiative lifetime depends mainly on the nature of the glass or crystal host.

2.2 Modeling

In the past decade, EDFAs have been well investigated by many different models in both steady and dynamic states. These models, which have various forms, can be applied to various EDFA applications under proper assumptions. Generally, we can divide them into two categories: *numerical models* [2.1-2.5] and *analytical models.* [2.6-2.9]

Numerical models solve the differential equations that are used to empirically describe the behavior of the EDFA. The numerical models include the three-level model and the two-level model. A homogeneous model assumes that all transitions are homogeneously broadened, i.e. all atoms in the host medium have the same laser line characteristics: center frequency, line width, peak cross-section, and fluorescence lifetime [2.5]. We choose a homogeneous two-level model for all simulations in this thesis.

The analytical model can simplify the differential equations to a transcendental equation under some assumptions by which many important parameters can be obtained analytically without complicated numerical calculations.

In this chapter, we will review the different models that are widely used to date and introduce our model for simulating gain-clamped L-band EDFAs.

2.2.1 Three-Level System for EDFAs

EDFAs can be described with a basic three-level atomic system as shown in Fig. 2.2 [2.1, 2.5, 2.10]. The three levels, ${}^4I_{15/2}$, ${}^4I_{13/2}$ and ${}^4I_{11/2}$ are denoted as the ground state, the metastable excited state and the excited state, respectively. As shown in Fig. 2.1, R_{13} is the pumping rate from the ground state ${}^4I_{15/2}$ to the high-energy level ${}^4I_{11/2}$ and R_{31} is the stimulated emission rate. However, the stimulated emission R_{31} is not the main process of erbium ions in the energy level ${}^4I_{11/2}$. The erbium ion decay or spontaneous emission from the excited state ${}^4I_{11/2}$ to ${}^4I_{13/2}$, which is denoted as A_{32}, is the dominant process, mainly caused by spontaneous nonradiative transitions.

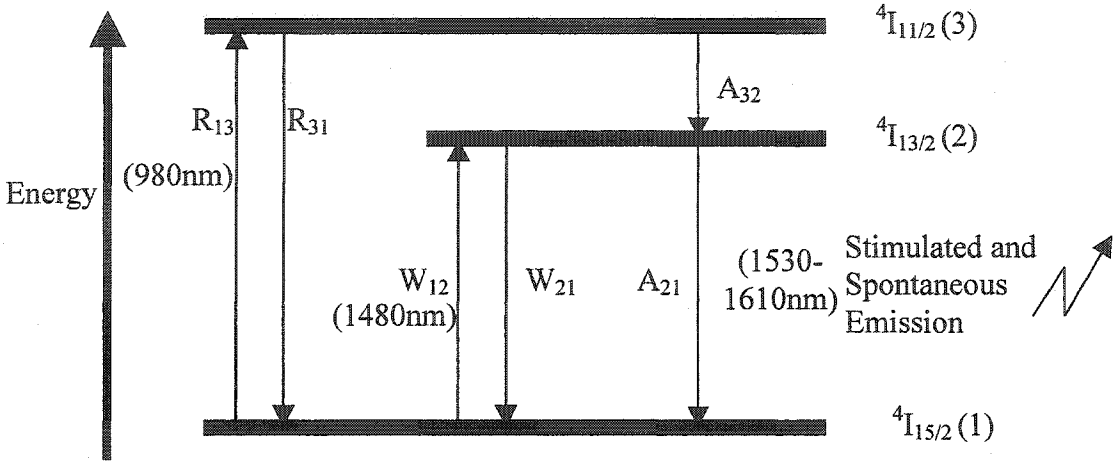

Fig. 2.2 A three-level system used for EDFA model

The stimulated absorption and emission rates between levels ${}^4I_{13/2}$ and ${}^4I_{15/2}$ are denoted as W_{12} and W_{21} while A_{21} represents the spontaneous emission. Here A_{21} is mainly decided by radiative decay and can be approximated as $A_{21} \approx 1/\tau$, where τ is the total lifetime. If we use N_1, N_2 and N_3 to represent the populations of the erbium ions in the three energy states ${}^4I_{15/2}$, ${}^4I_{13/2}$ and ${}^4I_{11/2}$, respectively, the rate equations for the three-level EDFA system can be written as follows:

$$\frac{\partial N_1}{\partial t} = -R_{13}N_1 + R_{31}N_3 - W_{12}N_1 + W_{21}N_2 + A_{21}N_2 \tag{2.4}$$

$$\frac{\partial N_2}{\partial t} = W_{12}N_1 - W_{21}N_2 - A_{21}N_2 + A_{32}N_3 \tag{2.5}$$

$$\frac{\partial N_3}{\partial t} = R_{13}N_1 - R_{31}N_3 - A_{32}N_3 \tag{2.6}$$

where $N_1 + N_2 + N_3 = N$ (the total erbium ion population).

2.2.2 Two-level System for EDFAs

2.2.2.1 Motivation

Although a three-level model can accurately describe the behavior of EDFAs, the complicated rate equations and numerous parameters bring a number of challenges for numerical simulations. On the other hand, it has been found that the decay of erbium ions from level ${}^4I_{11/2}$ to level ${}^4I_{13/2}$ is very fast (generally, the lifetime is between $1\mu s - 10\mu s$ depending on the fiber host type) while the lifetime of erbium ions in the metastable state is on the order of milliseconds, which is much longer than that in level ${}^4I_{11/2}$. The typical lifetime of the ${}^4I_{13/2}$ in various glass hosts is shown in Table 2.1. Since erbium ions that are pumped to level ${}^4I_{11/2}$ immediately decay to level ${}^4I_{13/2}$ in a very short time, N_3 can be considered zero and all excited erbium ions stay in the metastable state. Thus, we can use a two-level system to model an EDFA [2.1].

Host Glass	Lifetime (ms)
Na-K-Ba-silicate	14
Silicate	14.7
Al-P Silica	10.8
Al-Ge Silica	9.5
Fluorophosphate	8
Fluoride	10.3
Tellurite	4

Table 2.1: Lifetime of the ${}^4I_{13/2}$ level of Er^{3+} in various glass hosts [2.10].

The two-level model is accurate to predict the behavior of EDFAs when a 1480nm pump is used, in which only level ${}^4I_{15/2}$ and level ${}^4I_{13/2}$ are involved. For 980nm pumps, when

the pump power is less than 1W, the two-level model is still a good approximation due to the very short lifetime of erbium ions in level $^4I_{11/2}$ [2.3, 2.11].

2.2.2.2 General Model

With this simplification, a two-level EDFA model can be described by a group of rate equations and propagation equations. The rate equations are similar to the three-level system:

$$\frac{\partial N_1}{\partial t} = -W_{12}N_1 + W_{21}N_2 + A_{21}N_2 \tag{2.7}$$

$$\frac{\partial N_2}{\partial t} = W_{12}N_1 - W_{21}N_2 - A_{21}N_2 \tag{2.8}$$

where $N_1 + N_2 = N$ and $\frac{\partial N_2}{\partial t} = -\frac{\partial N_1}{\partial t}$

$$W_{12} = \sum_k W_{12}^k = \sum_k \frac{\sigma_a^k \Gamma_k P_k(z,t)}{Ah\nu_k} \tag{2.9}$$

$$W_{21} = \sum_k W_{21}^k = \sum_k \frac{\sigma_e^k \Gamma_k P_k(z,t)}{Ah\nu_k} \tag{2.10}$$

$$A_{21} = 1/\tau = \sum_j A_{21}^j = \sum_j \frac{\sigma_j^e \Gamma_j 2h\nu_j \Delta\nu_j}{Ah\nu_j} \tag{2.11}$$

where k represents the specified wavelength and σ_a^k and σ_e^k are absorption and emission cross-sections at wavelength k, respectively. P_k represents the field power at wavelength k. Γ_k is the overlap factor [2.3] and A is the effective cross-sectional area of the erbium ion distribution in the fiber. $2h\nu\Delta\nu$ is the equivalent noise power in a bandwidth $\Delta\nu$

corresponding to spontaneous emission [2.10]. In this model, N_2 is also called the upper state population or inversion level.

The propagation equations in the model are used to describe the power changes of signals, pumps and noise along the EDF. The change in the field power $dP_k(z,t)/dz$ (in the units of photons) is the net number of photons deposited or acquired in a length *dz* per unit time at time *t* [2.10] and hence, the propagation equations for signal/pump *(k)* and ASE noise *(j)* can be expressed as (2.12) and (2.13), respectively:

$$\frac{\partial P_k(z,t)}{\partial z} = W_{21}^k N_2(z,t) - W_{12}^k N_1(z,t) \tag{2.12}$$

$$\frac{\partial P_j(z,t)}{\partial z} = W_{21}^j N_2(z,t) - W_{12}^j N_1(z,t) + A_{21}^j N_2(z,t) \tag{2.13}$$

We normalize the total population so that $N_1 + N_2 = 1$, which means that the populations are considered on a per ion basis. Replacing W_{12}, W_{21} and A_{21} in (2.8), (2.12) and (2.13) with expressions (2.9), (2.10) and (2.11), the propagation equations for signal/pump and ASE noise can be written as (2.14) and (2.15), respectively:

$$\frac{\partial P_k(z,t)}{\partial z} = u\rho\Gamma_k\left[\left(\sigma_k^e + \sigma_k^a\right)N_2(z,t) - \sigma_k^a\right]P_k(z,t) \tag{2.14}$$

$$\frac{\partial P_j(z,t)}{\partial z} = u\rho\Gamma_j\left[\left(\sigma_j^e + \sigma_j^a\right)N_2(z,t) - \sigma_j^a\right]P_j(z,t) + uN_2(z,t)\sigma_j^e\Gamma_j 2h\nu_j\Delta\nu_j \tag{2.15}$$

where ρ is the erbium ion density. $u = +1$ or $u = -1$ is used to indicate the direction of propagation of the light beams. Based on the propagation equations, the rate equation can be expressed as:

$$\frac{\partial N_2(z,t)}{\partial t} = -\frac{N_2(z,t)}{\tau} - \frac{1}{\rho A}\left(\sum_{k,j}\left(\frac{\partial P_k(z,t)}{\partial z} + \frac{\partial P_j(z,t)}{\partial z}\right)\right) \tag{2.16}$$

The model described by equations (2.14-2.16) is the full model that can be used for any case. However, those partial differential equations must be solved in both the time domain and space domain simultaneously and therefore, complicated numerical methods are always needed, which can be very time-consuming.

2.2.2.3 Steady-State Model

The most important properties of an EDFA, such as signal gain and noise figure, can be obtained in the steady-state in which the populations and field powers along the EDF do not depend on time. With steady-state conditions, the upper state population does not change in time. Therefore, we can set the result of (2.16) to zero, i.e. $\frac{\partial N_2(z,t)}{\partial t} = 0$. N_2 can then be expressed as a function of signal, pump and noise field powers in the space domain. The steady-state EDFA model can be written as a set of coupled ordinary differential equations:

$$\frac{dP_k(z)}{dz} = u\rho\Gamma_k\left[\left(\sigma_k^e + \sigma_k^a\right)N_2(z) - \sigma_k^a\right]P_k(z) \tag{2.17}$$

$$\frac{dP_j(z)}{dz} = u\rho\Gamma_j\left[\left(\sigma_j^e + \sigma_j^a\right)N_2(z) - \sigma_j^a\right]P_j(z) + uN_2(z)\sigma_j^e\Gamma_j 2h\nu_j\Delta\nu_j \tag{2.18}$$

$$N_2(z) = -\frac{\tau}{\rho A}\left(\sum_{k,j}\left(\frac{dP_k(z)}{dz} + \frac{dP_j(z)}{dz}\right)\right) \tag{2.19}$$

To obtain static results, numerical solutions are still needed to solve equations (2.17-2.19). However, the calculation time is much shorter because ordinary differential equations are much easier to solve than partial differential equations.

2.2.3 Analytical Model

The analytical model was first developed by Saleh et al. [2.6] and so it is also called Saleh's model. This model, which involves only one simple transcendental equation, can predict signal gains and pump absorptions in the steady-state [2.6]. However, this model is only valid under the following assumptions: (1) the EDF is considered a two-level system; (2) the pump power is less than 1W; (3) excited-state absorption is absent; (4) homogeneous broadening [2.12]; and (5) the signal gain saturation by ASE noise is neglected, which means that the amplifier's gain should be less than about 20dB [2.6].

With the above assumptions, one transcendental equation can be derived from equation (2.14) and written as:

$$P_{out} = \sum_k P_k^{out} = \sum_k A_k e^{-B_k P_{out}} \tag{2.20}$$

where $A_k = P_k^{in} e^{-\alpha_k L} e^{P_{in}/P_k^{IS}}$, $B_k = \frac{1}{P_k^{IS}}$, $\alpha_k = \rho \Gamma_k \sigma_k^a$, and $P_k^{IS} = \frac{A}{\Gamma_k(\sigma_k^e + \sigma_k^a)\tau}$.

Since A_k and B_k are known, equation (2.20) can be solved for P_{out} and then P_k^{out} can be obtained for each wavelength. Although the power of the ASE noise cannot be obtained with (2.20), noise performance can also be modeled by analytical models [2.7,2.8].

One of the advantages of the analytical model is fast calculation speed, by which a lot of important amplifier properties, such as saturation power or pump gain threshold, can be obtained quickly. Although some assumptions are made in order to make the model valid, there are no approximations in reducing the differential equations to the transcendental equation. Therefore, the EDFA properties determined by this model should have good accuracy.

However, when the ASE noise generated in the amplifier is large enough to saturate the pump and gain, the analytical model will become inaccurate. In L-band EDFAs, ASE noise power is generally large due to the long length of EDF, which may have a large impact on signal gains and pump saturation. Therefore, analytical models are not suitable for simulating L-band EDFAs.

2.2.4 Gain-Clamped L-band Model

Gain-clamped EDFA models in the steady-state have been well investigated in the last few years [2.13-2.14]. In these models, the lasing signal in the amplifier, which is used to clamp the signal gains as described in sections 1.3.2 and 1.3.3, can be treated as a "normal" optical signal propagating in the amplifier, but with some special boundary conditions. An additional propagation equation for the lasing signal can be added to the homogeneous two-level numerical model described in equations (2.17-2.19):

$$\frac{dP_f^{\pm}(z)}{dz} = u\rho\Gamma_f\left[\left(\sigma_f^e + \sigma_f^a\right)N_2(z) - \sigma_f^a\right]P_f^{\pm}(z) \tag{2.21}$$

where f represents the wavelength of the lasing (feedback) signal. Although the initial value $P_f(0)$ and the boundary value $P_f(L)$ are both unknown, the propagation of P_f in the steady state is limited by the condition: $P_f(0) = P_f(L) * Loss$. Hence, it is not difficult to solve equation (2.21) with equations (2.14-2.16) simultaneously.

In the dynamic state, numerical models [2.15-2.18] and simplified models [2.19-2.21] in the C-band have been investigated by many research groups. These models are focused on the transient performance when the total input signal power changes, for example, as a result of channel add/drop operations or network reconfigurations. In this thesis, we extend the research to L-band EDFAs based on the full two-level dynamic model, which includes equations (2.14-2.16) and (2.21). However, our model is still based on a homogeneous system and an accurate all-optical L-band gain-clamped dynamic model that includes inhomogeneous effects such as spectral hole burning is still under investigation.

References

[2.1] J. R. Armitage, " Three-level fiber laser amplifier: A theoretical model," *Appl. Opt.*, vol. 27, no. 23, pp. 4831-4836, 1988.

[2.2] P. R. Morkel and R. I. Laming, "Theoretical modeling of erbium-doped fiber amplifiers with excited-state absorption," *Opt. Lett.*, vol. 14, no. 19, pp.1062-1064, 1989.

[2.3] C. R. Giles, E. Desurvire, "Modeling Erbium-Doped Fiber Amplifiers," *J. Light. Tech.*, vol. 9, no.2, pp. 271-283, 1991.

[2.4] E. Desurvire and J. R. Simpson, "Amplification of Spontaneous Emission in Erbium-Doped Single-mode Fibers," *J. Light. Tech.,* vol.7, no.5, pp.835-845, 1989.

[2.5] E. Desurvire, "Erbium-Doped Fiber Amplifiers-Principles and Applications," *John Wiley & Sons, Inc.* 1994.

[2.6] A.A.M. Saleh, R.M. Jopson, J.D. Evankow, Aspell, "Modeling of Gain in Erbium-Doped Fiber Amplifiers," *IEEE Photon. Lett.,* vol. 2, no.10, pp.714-718, 1990.

[2.7] R.M. Jopson and A.A.M. Saleh, "Modeling of gain and noise in erbium-doped fiber amplifiers," *SPIE* vol.1581, *Fiber Laser Sources and Amplifiers III*, 1991.

[2.8] I. Roudas, D.H. Richards, N. Antoniades, J.L. Jackel and R.E. Wagner, "An Efficient Simulation Model of the Erbium-Doped Fiber for the Study of Multiwavelength Optical Networks," *Optical Fiber Tech.* vol. 5, pp.363-389, 1999.

[2.9] T. Pfeiffer and H. Bulow, "Analytical Gain Equation for Erbium-Doped Fiber Amplifiers Including Model Field Profiles and Dopant Distribution," *IEEE Photon. Lett.,* vol. 4, no.5, pp.449-451, 1992.

[2.10] P.C. Becker, N.A. Olsson and J.R. Simpson, "Erbium-Doped Fiber Amplifiers-Fundamentals and Technology," *Academic Press,* 1997.

[2.11] Y. Sun, J.L. Zyskind and A.K. Srivastava, "Average Inversion Level, Modeling, and Physics of Erbium-Doped Fiber Amplifiers," *IEEE J. Sel. Topics in Quantum Electron.,* vol. 3, no.4, pp.991-1007, 1997.

[2.12] E. Desurvire, J.W. Sulhoff, J.L. Zyskind and J.R. Simpson, "Study of spectral dependence of gain saturation and effect of inhomogeneous broadening in erbium-doped

aluminosilicate fiber amplifiers," *IEEE Photon. Tech. Lett.,* vol. 2, no.9, pp.653-655, 1990.

[2.13] Y. Zhao, J. Bryce and R. Minasian, " Gain Clamped Erbium-Doped Fiber Amplifiers-Modeling and Experiment," *IEEE J. Sel. Topics in Quantum Electron.,* vol. 3, no. 4, pp.1008-1012, 1997.

[2.14] Haruo Okamura, "Automatic Optical Loss Compensation with Erbium-Doped Fiber Amplifier," *J. Light. Tech.*, vol. 10, no. 8, pp.1110-1116, 1992.

[2.15] K.Y. Ko, M.S. Demokan and H.Y. Tam, "Transient Analysis of Erbium-Doped Fiber Amplifiers," *IEEE Photon. Tech. Lett.,* vol. 6, no.12, pp.1436-1438, pp.1436-1438, 1994.

[2.16] D. H. Richards, J. L. Jackel and M. A. Ali, "A Theoretical Investigation of Dynamic All-Optical Automatic Gain Control in Multichannel EDFA's and EDFA Cascades," *IEEE J. Sel. Topics in Quantum Electron.,* vol. 3, no.4, pp.1027-1036, 1997.

[2.17] G. Luo, J.L. Zyskind, J.A. Nagel and M. A. Ali," Experimental and Theoretical Analysis of Relaxation-Oscillations and Spectral Hole Burning Effects in All-Optical Gain-Clamped EDFA's for WDM Networks," *J. Light. Tech.*, vol. 16, no. 4, pp. 527-533, 1998.

[2.18] Y. Sun, A.A.M. Saleh, J.L. Zyskind, D.L. Wilson, A.K. Srivastava and J.W. Sulhoff, "Time Dependent Perturbation Theory and Tones in cascaded Erbium-Doped Fiber Amplifier Systems," *J. Light. Tech.,* vol. 15, no.7, pp.1083-1087, 1997.

[2.19] K. Song, M. Premaratne and R.D. T. Lauder, "An Analytical Formulation of the Transient Response of Gain-Clamped EDFA's," *IEEE Photon. Tech. Lett.,* vol. 11, no. 11, pp.1378-1380, 1999.

[2.20] S.R. Chinn, "Simplified Modeling of Transients in Gain-Clamped Erbium-Doped Fiber Amplifiers," *J. Light. Tech.,* vol. 16, no.6, pp.1095-1100, 1998.

[2.21] Q. Yu and C. Fan, "Simple Dynamic Model of All-Optical Gain-Clamped Erbium-Doped Fiber Amplifiers," *J. Light. Tech.,* vol. 17, no.7, pp.1166-1171, 1999.

Chapter 3 Single-Stage Gain-Clamped L-Band EDFAs

We start by considering single-stage gain-clamped L-band EDFAs. Single-stage amplifiers are one of the basic amplifier structures in which only one coil of EDF is used. Many important parameters can be obtained from analysis of single-stage gain-clamped EDFAs in spite of its simple structure.

3.1 Configurations

We investigate two configurations of one-stage gain-clamped L-band EDFAs as shown in Fig. 3.1. The first configuration (denoted as Config 3-1) is a typical ring laser structure for all-optical gain clamping, which consists of a feedback loop to generate a laser signal. The other one (denoted as Config 3-2) incorporates a pair of FBGs to form an erbium-doped fiber grating laser (EDFGL).

Although both configurations incorporate fiber laser structures in the amplifiers to clamp the gain, there are still some differences between them. In Config 3-1, the feedback loop consists of taps, an optical filter and an optical attenuator and the feedback (lasing) signal can co-propagate or counter-propagate with the WDM signals. The total cavity loss is decided by two taps and the attenuator used in the feedback loop, which is generally larger than 10dB in order to minimize the loss of the output signal power. In Config 3-2, two lasing signals at the same wavelength exist simultaneously in the cavity and propagate opposite each other and the cavity loss is decided primarily by the reflectivities of the FBGs.

3.2 Simulation Model and Amplifier Parameters

3.2.1 Simulation Model

We simulate amplifier performance in the steady-state for both configurations using the two-level homogenous model discussed in Chapter 2. For simplicity, intricate effects such as excited-state absorption or inhomogeneous broadening are not considered because the related parameters are hard to obtain and furthermore, these effects will not have large impact on our simulations. To be exact, we use equations (2.17-2.19) and (2.21) to describe the propagation of signal, pump, ASE noise and lasing signals and also

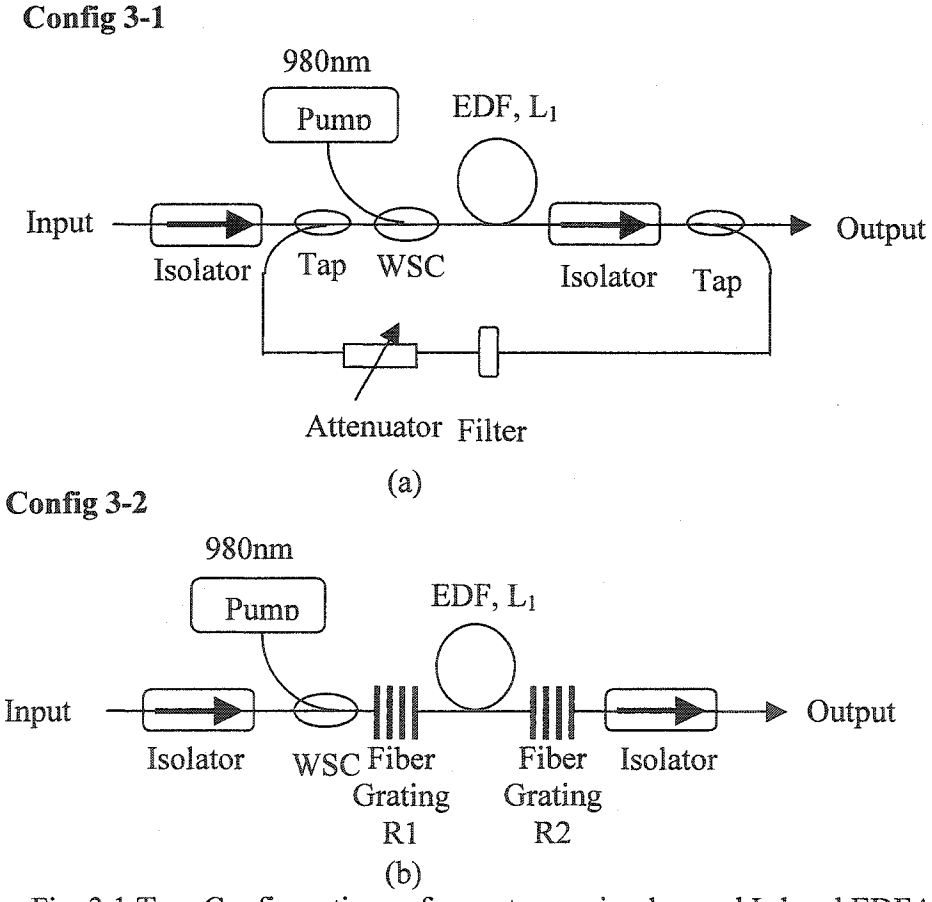

Fig. 3.1 Two Configurations of one-stage gain-clamped L-band EDFAs
(a) Config 3-1 (b) Config 3-2

the upper state population along the EDF. In order to calculate the ASE noise, the ASE noise spectrum is spectrally divided into many wavelength components with 1nm bandwidth in the region of 1450-1610nm and each optical bandwidth consists of forward and backward ASE noise. Therefore, we need 320 different equations to describe ASE noise, in which half of them are with initial conditions and half are with boundary conditions. Including the propagation equations for all signals and pump wavelengths, there are several hundred ordinary differential equations that are coupled together. We use a fourth order Runge-Kutta method and a shooting technique to solve all of the propagation equations and the population equation [3.1].

3.2.2 Amplifier Parameters

For experimental availability, we choose 100m of EDF and a 980nm co-propagating

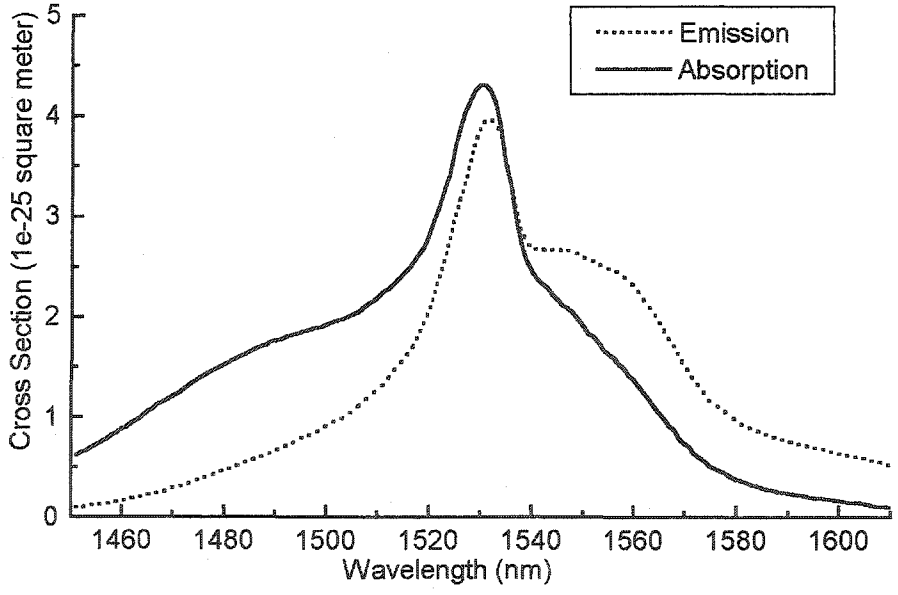

Fig. 3.2 Absorption (solid) and Emission (dotted) Cross Section for EDF used in the simulation

pump for both configurations. The EDF used in our model is a typical aluminum-germanium-erbium-doped silica fiber with absorption and emission cross-sections shown in Fig. 3.2, which is obtained from reference [3.2]. All other parameters of the EDF are given in Table 3.1.

Parameter	Value
Lifetime	10ms
Overlap Factor	0.4 for signals at 1450-1650nm 0.6 for pump at 980nm
Core Diameter (μm)	3
Effective Area (μm^2)	3.5
Erbium Concentration (ppm)	≈ 800

Table 3.1 Parameters of EDF used in simulations

Additionally, the optical filter, optical attenuator, tap, FBGs and isolator are assumed ideal (no insertion loss).

3.3 Simulation Results

3.3.1 Critical Power

In order to evaluate the gain-clamping effect, we define the critical power P_{crit} as a performance metric. The critical power is the maximum input signal power which causes the gain to decrease by 0.5dB from its maximum value in the small signal regime. When the input signal power exceeds P_{crit}, gain-clamping starts to fail. Hence, we can use the value of P_{crit} to evaluate the gain-clamping performance for any EDFA configuration. This definition is used in throughout the thesis as one of the most important performance metrics for gain-clamped EDFAs.

3.3.2 Config 3-1

First, we start by investigating Config 3-1. We set $\lambda_s = 1580nm$ (signal wavelength) and the pump power at 980nm to 100mW. The feedback level is chosen at 90%. For convenience, we use feedback level instead of the total cavity loss in the feedback loop. The feedback level represents the portion of output light that will be coupled back to the input via the feedback loop. For example, 90% feedback level means $P_f^{in} = P_f^{out} * 90\%$, which includes all losses from taps, the attenuator, etc.

Fig. 3.3 shows the signal gain as a function of the total input signal power at three different feedback wavelengths. The solid symbols represent the signal gain at the output and it can be noticed that the gain is quite small. This is because when the feedback level is 90%, 90% of the signal power at the output is also coupled to the feedback loop along with the feedback signal. If we can assume the optical tap used in Config 3-1 has

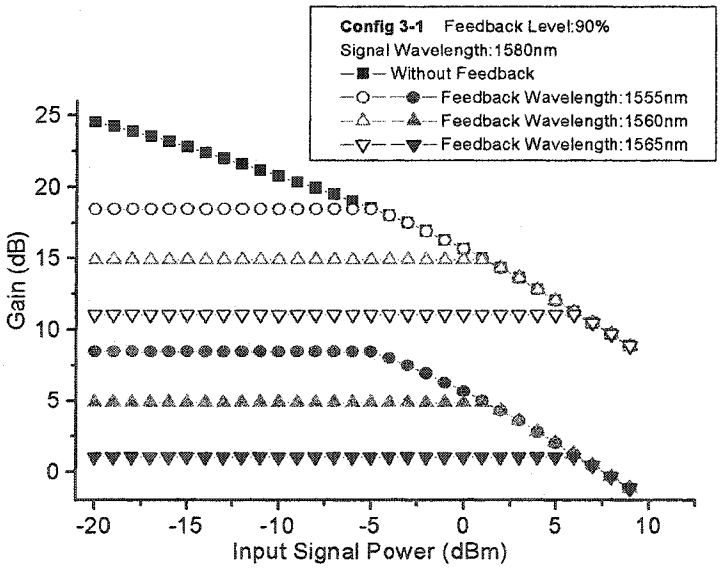

Fig. 3.3 Signal gain as a function of the total input signal power for the high feedback level for Config 3-1. $\lambda_s = 1580nm$, $L = 100m$, $P = 100mW$.

wavelength selectivity, i.e. only the signal at the feedback wavelength will be coupled to the feedback loop while all other optical signals will pass through, the real signal gains are shown as open symbols in Fig.3.3. It is clearly seen that the solid symbols are 10dB lower than the open symbols. Hence, the application of Config 3-1 with high feedback level is impractical due to the low gain for signal wavelengths.

For a low feedback level (e.g. 5%), Config 3-1 achieves good gain performance as shown in Fig 3.4. High gains and also large critical powers can be obtained: $G = 19dB$ with $P_{crit} = -7dBm$ for $\lambda_f = 1555nm$; $G = 16.5dB$ with $P_{crit} = -2dBm$ for $\lambda_f = 1560nm$ and $G = 15dB$ with $P_{crit} = +2dBm$ for $\lambda_f = 1565nm$.

We also simulate the noise performance for different feedback conditions as shown in Fig 3.5. We use (3.1) to calculate the NF:

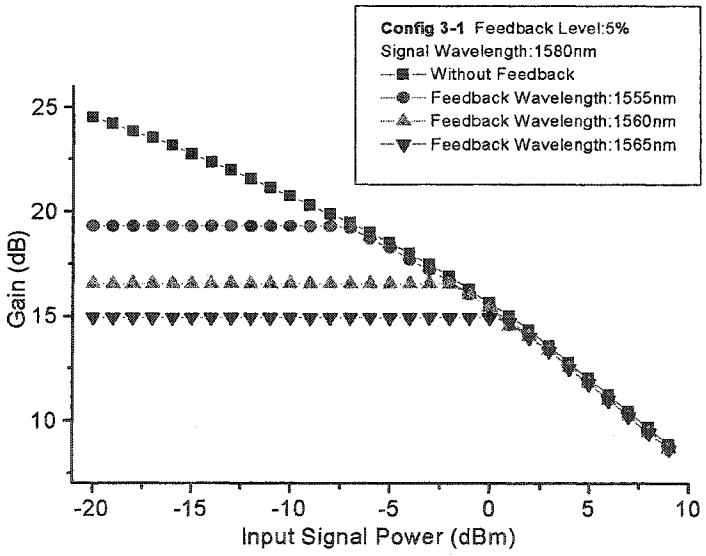

Fig. 3.4 Gain as a function of input signal power for the low feedback level for Config 3-1. $\lambda_s = 1580nm$, $L = 100m$, $P = 100mW$.

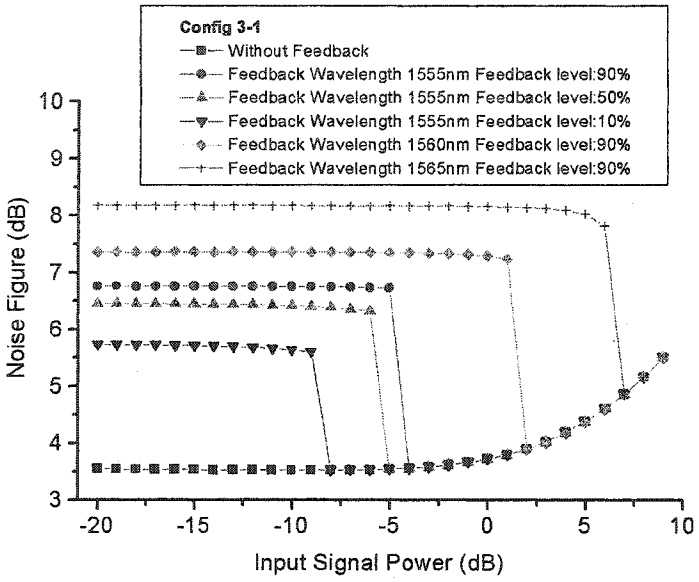

Fig. 3.5 Noise Figure as a function of input signal power for different feedback conditions. $\lambda_s = 1580nm$, $L = 100m$, $P = 100mW$.

$$NF = \frac{P_{ASE}}{h\nu \cdot \Delta\nu \cdot G} + \frac{1}{G} \tag{3.1}$$

where G and P_{ASE} are gain and noise power at λ. $h\nu$ is the photo energy and $\Delta\nu$ is the bandwidth of noise. Although the tap used at the output decreases the gain, the NF is not affected since the ASE noise powers are also attenuated [3.3]. As can be seen in Fig. 3.5, the lowest NF (5.8dB) is obtained with the lowest feedback level (10%). Furthermore, a high feedback level with a long feedback wavelength leads to the highest NF $\approx$8.2dB.

3.3.3 Config 3-2

Config 3-2 uses a pair of FBGs to form an EDFGL in the amplifier in order to clamp the gain. An FBG is a band-pass reflector in which an optical signal centered at the Bragg wavelength will be reflected; other wavelengths, however, will be transmitted through the

FBG. Hence, no matter what the feedback level we use, signals (other than feedback wavelength) will be transmitted through the FBG without power loss at the output. Compared to Config 3-1, this configuration is more flexible in adjusting the feedback wavelength and feedback level to obtain a better performance of gain-clamped EDFAs. Since the lasing signal propagates in the cavity back and forth, the simulations are more complicated than in Config 3-1. An additional equation for the backward propagation of the lasing signal is required. Furthermore, the feedback level of the cavity is mainly determined by the FBG reflectivities R_1 and R_2.

3.3.3.1 Signal Gain and Noise Figure

(1) Feedback Wavelength

We also set the feedback level $\approx 90\%$ by using $R_1 = 99.9\%$ and $R_2 = 90\%$ (R denotes

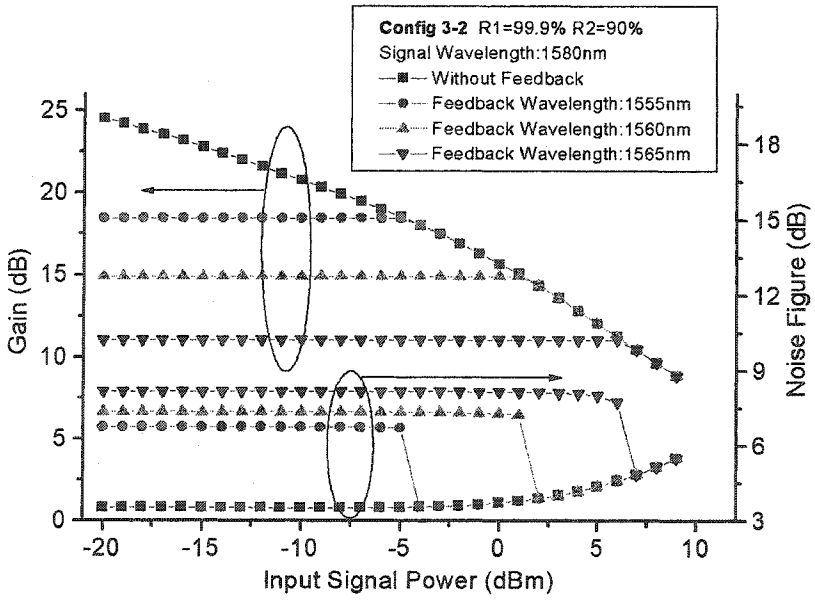

Fig. 3.6 Gain and NF as a function of input signal power for three feedback wavelengths for Config 3-2. $\lambda_s = 1580nm$, $L = 100m$, $P = 100mW$.

the reflectivity of an FBG) and the pump power at 980nm is 100mW. To see the impact of the feedback wavelength on the amplifier, we first simulate the signal gain and NF for three different feedback wavelengths. As shown in Fig. 3.6, 18dB gain and $P_{crit} = -5dBm$ are obtained when the feedback wavelength is far from the signal wavelength ($\lambda_f = 1555nm, \lambda_s = 1580nm$). When we increase the λ_f to 1560nm and 1565nm, the signal gains decrease to 15dB and 11dB, respectively, with the critical power improving to +1dBm and +6dBm, respectively. It is clear that different feedback wavelengths can change the signal gain level as well as P_{crit}. In Fig 3.6, the square line represents the signal gain without feedback. We show this curve in order to explain the maximum P_{crit} we can achieve at one gain level. For example, if the expected signal gain is 20dB, the maximum P_{crit} will be around –8dBm from the Fig. 3.6 since the signal output power in the gain-clamped case cannot exceed that in the unclamped situation.

Next, we consider the noise performance of Config 3-2. Fig.3.6 shows the NFs as a function of the input signal power for different feedback wavelengths. When the input signal power is less than P_{crit}, the NF is clamped as well as the signal gain. This feature is very useful since we can easily predict the performance of the system with clamped gain and NF. However, the clamping structure leads to a degradation of the NF. There is an increase of a few dB in the NF of the clamped structures compared to the conventional structure without clamping. Furthermore, the feedback wavelength also has some impact on NF. As can be seen in Fig 3.6, there is a little degradation of NF (around 1.5dB) when λ_f increases from 1555nm to 1565nm, possibly due to the smaller gain at $\lambda_f = 1565nm$.

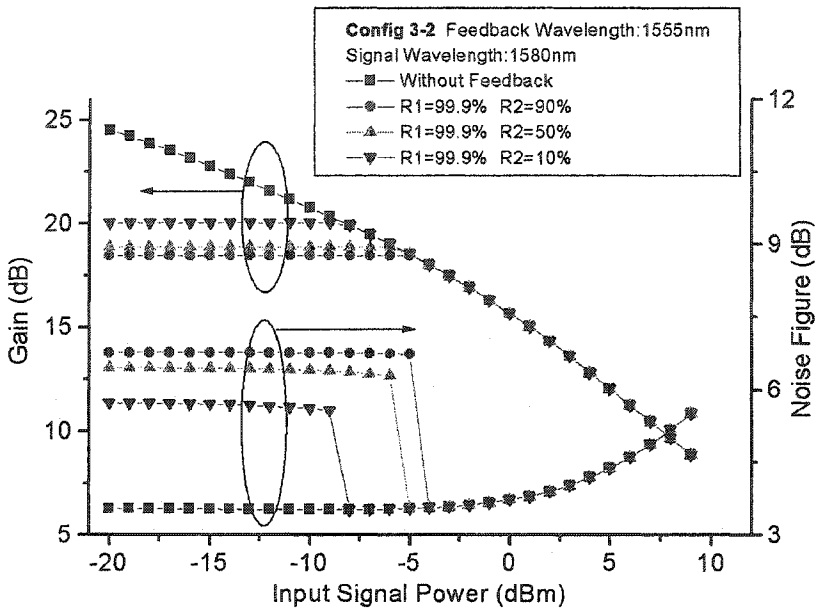

Fig. 3.7 Gain and NF as a function of input signal power for three different feedback levels for Config 3-2. $\lambda_s = 1580nm$, $L = 100m$, $P = 100mW$.

(2) Feedback Level

We have seen the impact of the feedback wavelength on the properties of Config 3-2. Next we study the performance of Config 3-2 for different feedback levels. The pumping conditions are the same as before and $\lambda_f = 1555nm$ and $\lambda_s = 1580nm$. The results are shown in Fig. 3.7.

As can be seen, when R_2 decreases from 90% to 10%, the signal gain increases from 18dB to 20dB, but the critical power shrinks from –5dBm to -7.5dBm. This result is similar to that of changing the feedback wavelength as shown in Fig.3.6.

For noise performance, we can see the NFs are fixed when $P_s < P_{crit}$ for each case, which means that the NFs are also clamped. Second, we find that a lower feedback

level results in a better NF. When $R_2 = 10\%$, the NF is lowered to around 5dB compared to 7dB at $R_2 = 90\%$. This NF improvement is mainly due to the smaller reflectivity of R_2, which leads to a different distribution of N_2 in the EDF and hence NF.

(3) Pump power and P_{crit}

Both the feedback wavelength and level can adjust the gain level, but as the gain increases, P_{crit} becomes smaller when the pumping condition is unchanged. Since the critical power is also an important parameter for a gain-clamped amplifier, we further investigate impact of the pumping condition on P_{crit}. We fix the feedback wavelength $\lambda_f = 1555nm$ and the feedback level $R_1 = 99.9\%, R_2 = 90\%$, and then simulate the signal gain for different pump powers from 70mW to 120mW. Fig 3.8 shows the signal

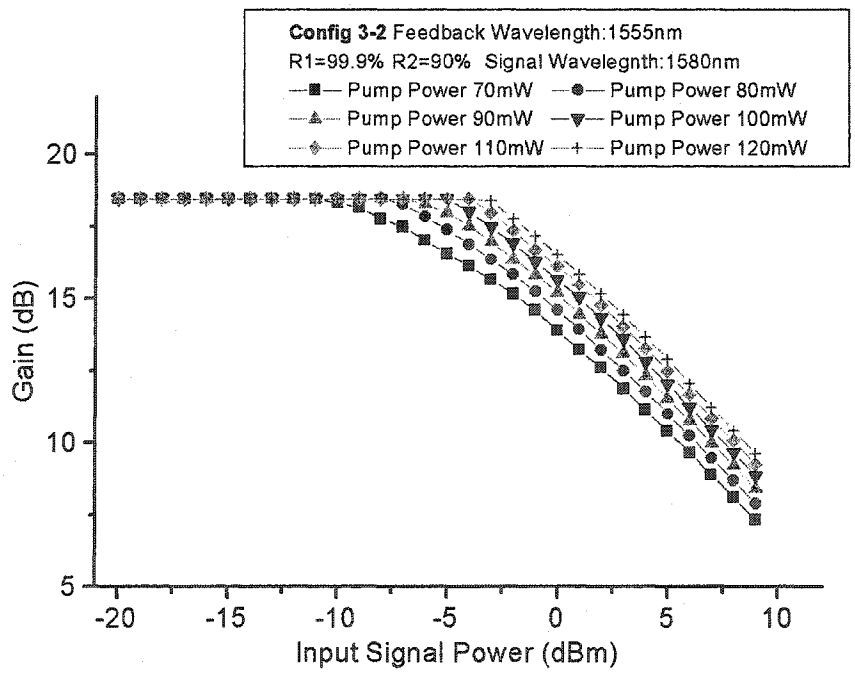

Fig. 3.8 Gain as a function of input signal power for different pump powers. $\lambda_s = 1580nm$, $L = 100m$.

gain as a function of input signal power for 6 different pump powers at $\lambda_s = 1580nm$. There are two observations: (i) the signal gain level in the clamping state does not change as pump power increases; (ii) the critical power varies as pump power changes with a larger P_{crit} achieved by higher pump powers. It is clear that the signal gain is not affected by variations of the pump power or the input signal power in a gain-clamped EDFA as long as clamping exists; this is different from a conventional EDFA. Fig. 3.9 represents the curves of P_{crit} as a function of pump power. It can be seen clearly that P_{crit} increases with increasing pump power regardless of the feedback conditions. Hence, we can use both the feedback wavelength and the feedback level to adjust the gain level and noise figure, and then change the critical power to the desired level by increasing the pump power. In such a way, high-gain, low NF and also high critical power for a specific λ can be easily obtained with Config 3-2.

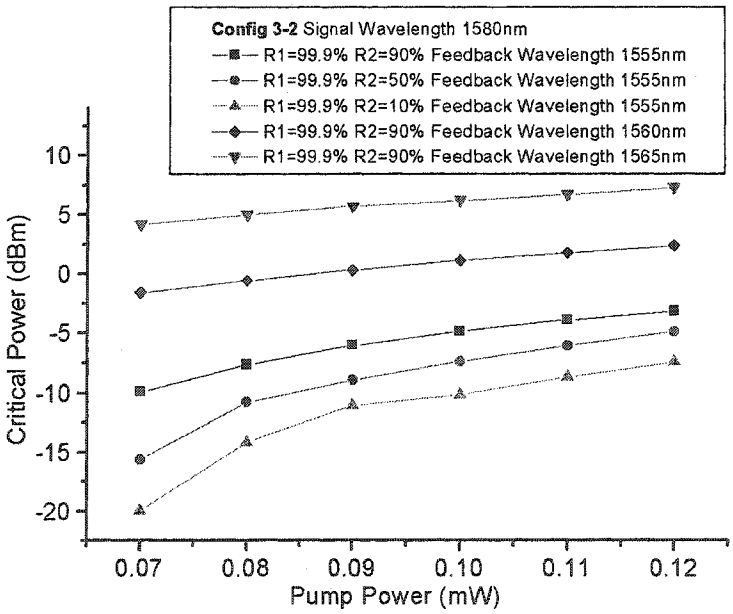

Fig. 3.9 Critical power as a function of pump power for different combinations of the feedback wavelengths and the feedback levels for Config 3-2, $\lambda_s = 1580nm$, $L = 100m$.

3.3.3.2 Gain and NF Spectra

(1) Gain Spectrum

The gain spectrum is very important for an EDFA that will be used in a multi-channel system. Since the gain of an EDFA is very sensitive to the wavelength of the input signal, the signal output power may be very different for two different channels even if the input power per channel is the same. In a long-haul system, this gain difference will accumulate along the transmission spans, eventually degrading system performance. Therefore, the gain spectrum of EDFAs needs to be investigated carefully.

Since the amplifier is gain-clamped, gain spectrum is fixed as long as the total input signal power is less than P_{crit}. We set the input signal power to –20dBm randomly and simulate the gain spectrum for Config 3-2 in the region of 1550-1610nm as shown in Fig 3.10 (a). It can be seen that the square line which represents the gain spectrum of the

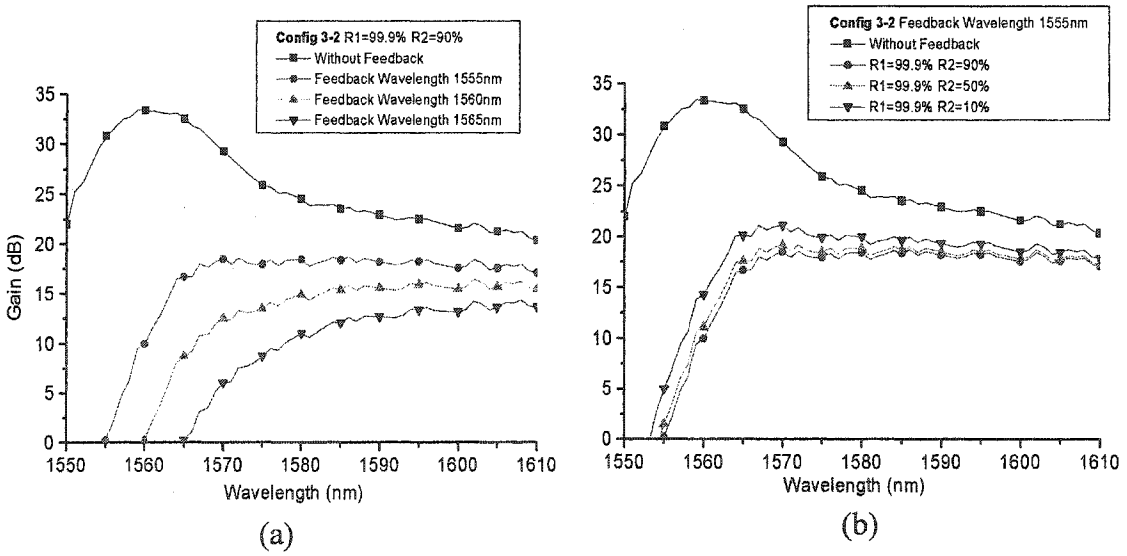

Fig. 3.10 Gain spectra for Config 3-2. Input signal power =-20dBm, $L = 100m$, $P = 100mW$. (a) for different feedback wavelengths (b) for different feedback levels

case without clamping, shows quite a large gain fluctuation over the whole L-band and the maximum gain variation is approximately 8dB. Although we can optimize the pumping condition to achieve a smaller gain variation for a conventional EDFA without clamping, the new gain spectrum may tilt again when the input signal power changes since the gain is dependent on the total input signal power as shown in Fig. 3.6 and Fig. 3.7.

With the gain-clamping structure, the gain spectrum is fixed even if the input signal power or pump power changes as long as clamping does not fail. As shown in Fig. 3.10(a), the gain spectrum can be tilted by changing the feedback wavelength. The circle line with feedback wavelength at 1555nm shows high gain (approximately 18dB) and very small gain variation (<1dB). In this figure, we can also see that the gain at 1555nm of the circle line is just above 0dB for the clamped structure and that there is no gain for wavelengths shorter than 1555nm whereas the level of the square line at 1555nm is more than 30dB for the conventional structure. That is to say the feedback (lasing) signal at 1555nm suppresses the gains at shorter wavelengths and effectively changes the shape of the gain spectrum in the longer wavelength region.

Fig. 3.10(b) shows the simulation results of the gain spectra of Config 3-2 for different feedback levels. The feedback levels are set to $R_2 = 90\%, R_2 = 50\%$ and $R_2 = 10\%$. The gain spectrum can also be altered by different feedback levels. When we change R_2 from 90% to 10%, the gain spectrum raises approximately 2dB and the gain variation over L-band becomes 2dB. Although the change of gain spectrum by different feedback levels is not so large, it provides another method to tilt the gain spectrum.

Furthermore, we can adjust the feedback wavelength and the feedback level at the same time to achieve a very flat gain spectrum.

(2) NF Spectrum

The NF spectrum is as important as the gain spectrum in a multi-channel system. The NF may vary at different wavelengths and furthermore, it is only partly related to the signal gain. Other parameters such as the distribution of N_2 along the EDF are more critical to determine the NF. For example, even if we achieve a very flat gain spectrum with a high gain level, it does not mean that a flat NF spectrum with a low NF level can be obtained automatically. In a gain-clamped EDFA, the situation becomes more complicated since the feedback wavelength and the feedback level in the amplifier may have a large impact on the NF and NF spectrum. Therefore, the NF also needs to be studied carefully in gain-clamped configurations.

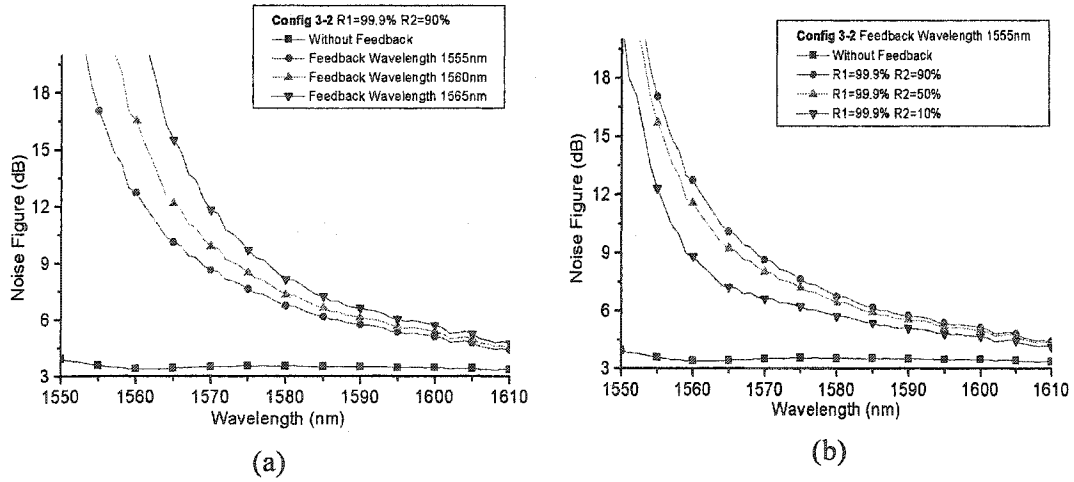

Fig. 3.11 Noise Figure spectra for Config 3-2. Input signal power =-20dBm, , $L = 100m$, $P = 100mW$. (a) for different feedback wavelengths (b) for different feedback levels.

As for Config 3-2, we simulate the NF spectrum for the following two cases: (1) the feedback wavelength varies but the feedback level is fixed; (2) the feedback level changes but the feedback wavelength is fixed. Fig. 3.11(a) summarizes the results for the first situation. As can be seen, the square line represents the NF spectrum of the conventional case, which is very flat while its corresponding gain spectrum varies significantly (8dB fluctuation). The circle line, which represents the case with 1555nm feedback wavelength, shows a large NF variation, especially from 1570-1585nm (here we just discuss about L-band wavelength from 1570nm-1610nm) even though the corresponding gain spectrum is very flat as seen in Fig 3.10(a). The NF is 9dB at 1570nm and 6.5dB at 1585nm. When the feedback wavelength is changed to 1565nm, we obtained the worst NF spectrum, possibly due to the longest feedback wavelength we select and its small corresponding gain. The NF degrades to 12dB at 1570nm and 7.5 dB at 1585nm, which makes these wavelengths unavailable to be used in most applications in long-haul transmission systems. Therefore, the feedback wavelength is not very effective to lower the NF although it is useful to tilt the gain spectrum as shown before.

Fig 3.11 (b) shows the NF spectra for different feedback levels when the feedback wavelength is fixed to 1555nm. The inverted-triangle curve shows the best NF spectrum, especially from 1570-1585nm. We can see the NF at 1570nm is lowered to 6.5dB and 5.5dB at 1585nm. A few dB improvement of NF is obtained by simply changing the feedback level from 90% to 10%. The reason that the lower feedback level can lead to a better noise performance is that the feedback level is the key parameter to decide the distribution of N_2 in a gain-clamped EDFA.

(3) Upper State Population (Inversion Level)

In order to understand the impact of feedback conditions on the upper state population, we show the distribution of N_2 along the EDF for different feedback wavelengths and different feedback levels, see Fig 3.12 and Fig 3.13. As shown in Fig.3.12, the distribution of N_2 for the conventional case is quite high in the first 20m of EDF and gradually decreases along the rest of fiber. It is well known that a low NF is obtained if the pump power is fully inverted in the front part of EDF and the upper state population is very high in the front part of the EDF [3.4]. Thus, a low NF can be achieved for the conventional case (around 3.5dB at 1580nm).

In the case with gain-clamping, the distributions of N_2 for three feedback wavelengths are flat over the entire EDF except the portion of the first 10m EDF. This can explain the degradation of NF spectrum in a gain-clamped EDFA. Furthermore, we

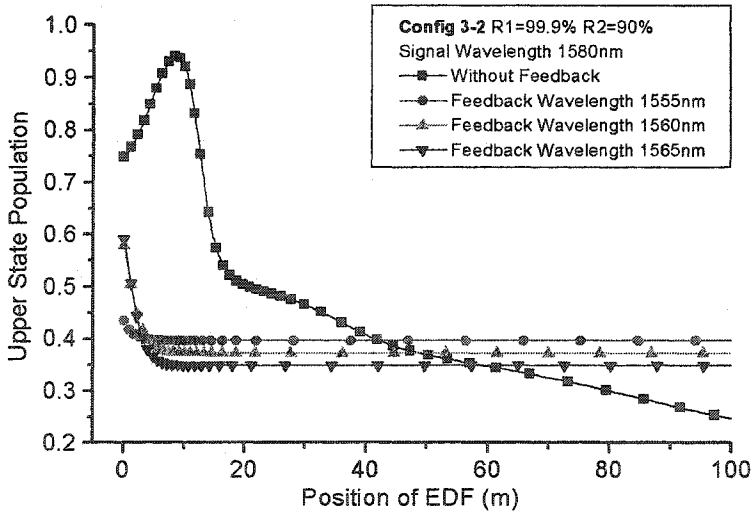

Fig. 3.12 Distribution of upper state population along the EDF for different feedback wavelengths. Input signal power =-20dBm, $L = 100m$, $P = 100mW$.

can see that when the feedback wavelength changes, the main level of the distribution curve varies which leads to a decrease in the average inversion level (N_2). We have introduced the inversion level in Chapter 1 and Fig 1.3 shows that the signal gain is decided by the average inversion level. Therefore, different feedback wavelengths result in variations of the average inversion level and hence gain. This can be used to explain why the feedback wavelength has a large impact on the signal gain.

Fig 3.13 shows the distribution of N_2 for different feedback levels. It is found that using a different feedback level can change the distribution of N_2 in the front portion of EDF (0-10m). Furthermore, the distribution of N_2 for the rest of EDF is almost unchanged. Hence, the average inversion level will not be altered to a significantly new level when the feedback level changes. As can be seen in Fig 3.7, we showed the signal gain at 1580nm varies from 18dB to 20dB when the feedback level decreases from 90%

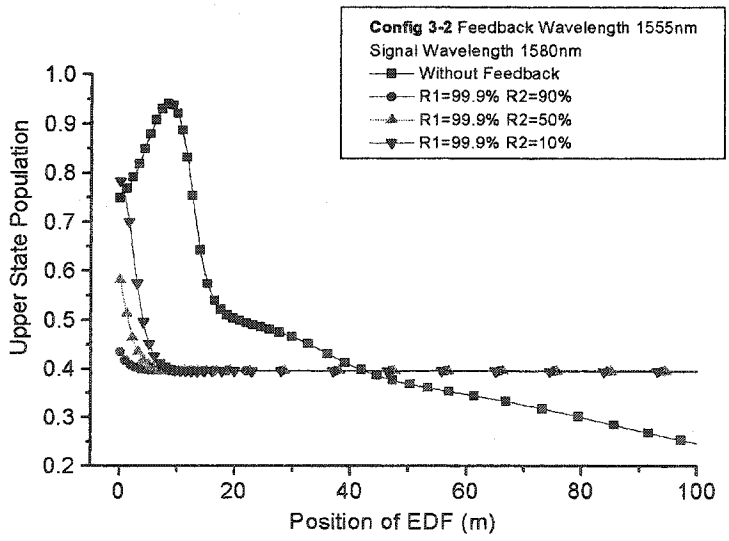

Fig. 3.13 Distribution of upper state population along the EDF for different feedback levels. Input signal power =-20dBm, $L = 100m$, $P = 100mW$.

to 10%. However, the distribution change in the front 10m of EDF is very important for noise performance. When we set $R_2 = 10\%$, a significant NF improvement is obtained compared to the case of $R_2 = 90\%$; the NF at 1580nm decreases from 7dB to 5dB.

From above figures, we understand that the feedback wavelength is effective in adjusting the gain level and a lower feedback level can greatly improve the noise performance. Hence, we can use both feedback conditions to optimize the configuration of a gain-clamped EDFA to achieve high gain, low NF and flat gain spectrum. Since the pump power does not affect the gain and NF in a gain-clamped amplifier (it affects primarily the critical power), the optimization process for gain and NF becomes simple and straightforward.

3.4 Discussion

3.4.1 Feedback Levels of R_1 and R_2 in Config 3-2

In the above discussion of Config 3-2, we always set $R_1 = 99.9\%$ and change R_2 to adjust the feedback level. However, we can also fixed R_2 to 99.9% and vary R_1 to a different level to alter the overall feedback level. In such a way, the lasing signal will get out of cavity in the opposite direction of the signals. We denote this configuration as Config 3-2-1.

We investigate Config 3-2-1 and compare the result with Config 3-2. As shown in Fig. 3.14, the gains for both configurations are exactly same at the same feedback conditions and their corresponding critical powers are the same. We also find in our

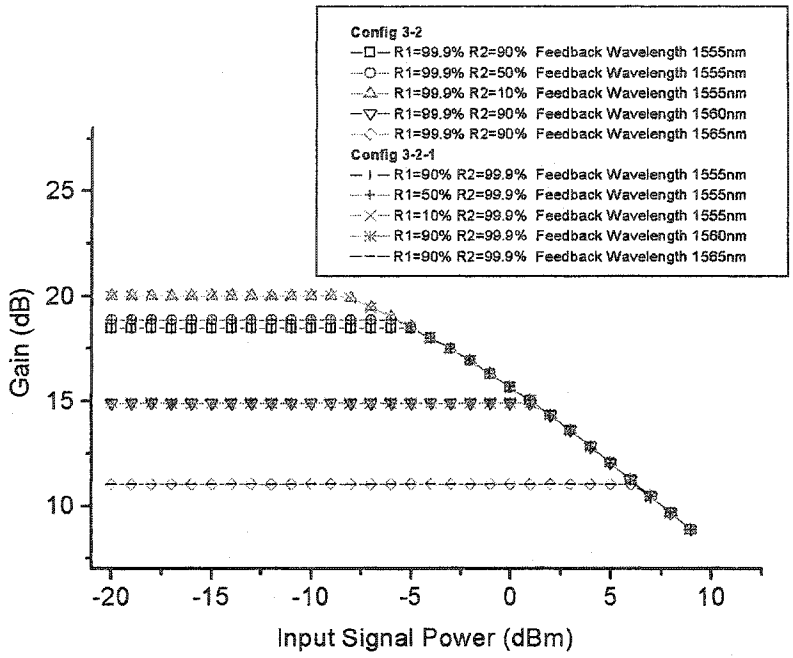

Fig. 3.14 Gain as a function of input signal power for Config 3-2 and Config 3-2-1. $\lambda_s = 1580nm$, $L = 100m$, $P = 100mW$.

simulations that noise performances in Config 3-2 and Config3-2-1 are almost the same. Hence, we can change the position of R_1 and R_2 without affecting any performance of the amplifier.

For a single-stage gain-clamped amplifier, when we choose the structure of Config 3-2-1, the lasing signal will disappear at output of the amplifier since R_2 is close to 100%. Most of the lasing output will emit from R_1 and counter-propagates along the fiber. This lasing power will meet the isolator placed at input side (see Fig. 3.1(b)) and is eventually absorbed. Therefore, there will be no lasing power leaking outside the gain-clamped EDFA of Config 3-2-1.

For a two-stage EDFA, Config 3-2 is more useful since we can make use of the lasing output power. If we use Config 3-2 as the first stage of a two-stage amplifier, the

lasing output will enter the second stage and suppress the gain in the second stage, which clamps the overall gain of the amplifier. Further discussion will be seen in the next chapter.

3.4.2 Comparison of Config 3-1 and Config 3-2

We have shown simulation results for both Config 3-1 and Config 3-2 in section 3.3.2 and section 3.3.3. The final results are very close for both configurations depending on the feedback level. The critical power and NFs can be obtained with the same feedback conditions and pumping conditions. We list the signal gain, noise figure and the critical power for both configurations in Table 3.2.

		Config 3-1			Config 3-2		
Feedback Wavelength	Feedback Level	Gain	NF	P_{crit}	Gain	NF	P_{crit}
1555nm	90%	8dB	6.7dB	-5dBm	18dB	6.7dB	-5dBm
1560nm	90%	5dB	7.3dB	+2dBm	15dB	7.3dB	+2dBm
1565nm	90%	2dB	8.2dB	+6dBm	12dB	8.2dB	+6dBm
1555nm	50%	15.8dB	6.4dB	-6dBm	18.8dB	6.4dB	-6dBm
1555nm	10%	20dB	5.7dB	-9dBm	20dB	5.7dB	-9dBm

Table 3.2 Comparison of Config 3-1 and Config 3-2 for gain, NF and P_{crit}

We can conclude Config 3-1 and Config 3-2 have the same noise performance and the critical power when the feedback conditions are the same. For a low feedback level, the two configurations even show very similar gains. However, when a high feedback level is required, especially for the two-stage EDFA structures we propose in the next chapter, Config 3-2 shows advantages over Config 3-1 in terms of the gain

performance. Although 90% feedback level is not practical in a single-stage gain-clamped EDFA due to the bad noise performance, it can be very useful in a two-stage gain-clamped amplifier. Moreover, all-optical gain-clamped amplifiers with high feedback levels show significant improvement in their dynamic performance. This is because the lasing can be built very quickly in the cavity due to the very strong feedback. Therefore, when the input signal power changes, the lasing can be rebuilt in a short time, which dramatically reduces the transient time. In Chapter 4, we will show how we can benefit from using FBGs with high feedback level in our two-stage gain-clamped amplifiers in steady state. In Chapter 5, we will discuss the dynamic performance of these gain-clamped amplifiers.

References

[3.1] H. Willams, "Numerical Recipes in C: the art of scientific computing," *Cambridge [England], New York, NY, USA, Cambridge University Press*, 1992.

[3.2] P.C. Becker, N.A. Olsson and J.R. Simpson, "Erbium-Doped Fiber Amplifiers-Fundamentals and Technology," *Academic Press,* 1997.

[3.3] J. Massicott, C. Lebre, R. Wyatt, R. Kashyap, D. Williams and A. Yu, "Low noise, all-optical gain controlled Er3+ doped fiber amplifier using asymmetric control laser cavity design," *Electron. Lett.*, vol.32, no.9. pp. 816-817,1996.

[3.4] E. Desurvire, "Erbium-doped Fiber Amplifiers-principles and applications," *John Wiley & Sons, Inc.* 1994.

Chapter 4 Two-Stage Gain-Clamped L-band EDFAs

4.1 Introduction

An L-band EDFA usually needs a long coil of EDF in order to obtain high gain due to the small emission cross section at L-band wavelengths. In the previous chapter, we showed that with single-stage structures, high gain and flat gain spectrum can be obtained with proper feedback conditions. However, it can be seen in Fig. 3.11 that NFs are obviously degraded compared with the conventional EDFAs without gain-clamping. Furthermore, with single-stage structures, forward and backward ASE noise are generated and well amplified along the long coil of EDF and eventually saturate the amplifier, which greatly decreases the power conversion efficiency [4.1].

It has been shown that a two-stage structure for EDFAs with an isolator in the middle will greatly improve the gain and noise performance [4.2, 4.3]. With a midway isolator, although the forward ASE noise is not affected, a significant portion of the backward ASE is eliminated, which saves more upper state population for amplification of the signal. Therefore, two-stage structures are widely used in L-band EDFAs.

In the previous chapter, we demonstrated two single-stage structures of gain-clamped L-band EDFAs: the ring laser configuration that uses a ring laser in the system via a feedback loop and the FBG configuration that incorporates a pair of FBGs on both ends of the amplifier to form an EDFGL. For two-stage EDFAs, the ring feedback configuration can also be formed to clamp the gain by simply adding the feedback loop to the system. However, the FBG configuration is not applicable to a two-stage amplifier with an isolator in the middle: an EDFGL cannot be formed if we place a pair of FBGs on

both ends of the ampifier since the light is only allowed to propagate in one direction due to the isolator used in the structure.

Recently, it has been shown that EDFAs with gain-clamped characteristics can be obtained in two-stage amplifier designs using partial gain-clamping, i.e. only one stage is truly gain-clamped but the overall gain-clamping effect is nevertheless achieved. Inoue [4.4] demonstrated that the noise figure (NF) of a gain-clamped C-band EDFA using a counter-propagating ring resonator can be reduced by using a short length of EDF (that does not cause gain saturation) for pre-amplification. For L-band EDFAs, Mahdi et al. showed that by incorporating a ring-laser in the first stage, an overall gain-clamping effect can be achieved [4.5], although the authors' intention in the paper was to demonstrate the use of a signal-seeding technique.

Based on these efforts, we propose two configurations for two-stage L-band EDFAs with gain-clamped characteristics based on partial gain-clamping. Both configurations are based on the FBG configuration that was discussed in the previous chapter, but only one stage is truly clamped. In the following sections of this chapter, we will investigate theoretically and experimentally the properties of the partially clamped EDFAs that we propose.

4.2 Configuration

The two L-band EDFA configurations that we investigate are shown in Fig. 4.1. In the first configuration (denoted Config 4-1), a pair of FBGs is deployed on both sides of the EDF in the first stage, forming an EDFGL to clamp the gain in the first stage. The

second stage is a conventional stage without any special structure for clamping. This configuration is similar to that proposed by Mahdi and Ahmad [4.5]; however, we use an EDFGL rather than a ring laser in the first stage. The advantage of our EDFGL configuration is that by using wavelength selective FBGs having different reflectivities, we can easily control the power of the feedback signal exiting the first stage without affecting the power of the signal wavelengths. In the second configuration (denoted Config 4-2), the FBGs are moved to the second stage where the EDFGL is formed.

Both configurations are partially gain-clamped. The only physical difference between them is the stage in which the EDFGL is formed. However, by varying the stage which is gain-clamped, the underlying principles of operation for achieving the overall gain-clamping effect are very different. In Config 4-1, the EDFGL clamps the gain in the first stage and also generates a seed signal to the second stage. This seed signal automatically compensates the total signal power injected to the second stage, i.e. when some channels are added/dropped, the power of the seed signal decreases/increases, and hence the signal gains after the second stage show gain-clamped characteristics. The seed signal is the key to obtain the overall gain-clamped performance.

Config 4-1

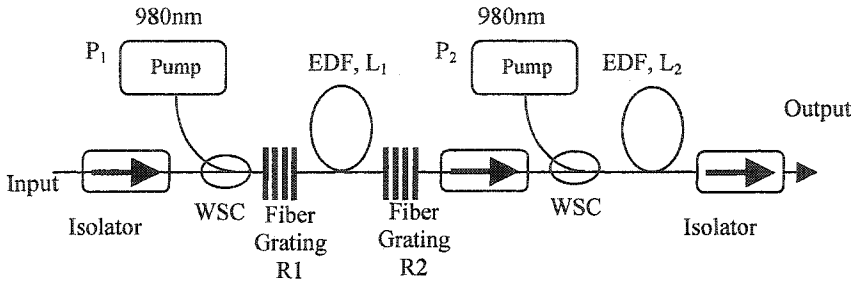

Config 4-2

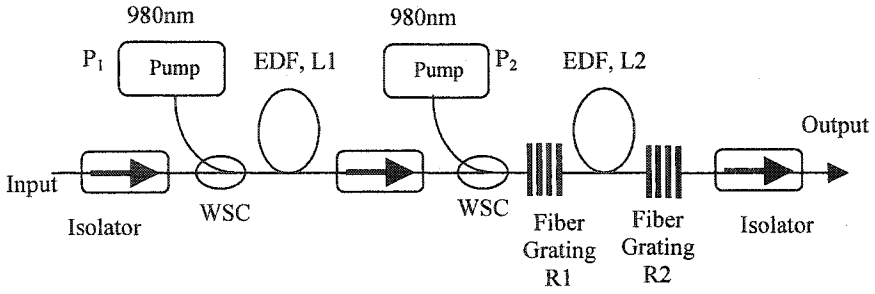

Fig. 4.1 Two Configurations of partially gain-clamped two-stage L-band EDFAs. EDF: erbium-doped fiber; WSC: wavelength selective coupler.

In Config 4-2, the first stage works as a preamplifier but in the unsaturated regime. Since the signal gains for L-band wavelengths in the first stage are normally very small due to the short EDF length and small emission and absorption cross-sections at these wavelengths (between 2-7dB depending on the wavelength), the first stage can be kept far from gain saturation and exhibits fixed gain performance. The second stage behaves as a gain-clamped booster to provide high gains for L-band signals and also gain-clamping effect. Table 4.1 summarizes the functions of each stage for both configurations in achieving overall gain-clamped characteristics.

	Functions of the first stage	Functions of the second stage
Config 4-1	(1) Clamps the signal gains in the first stage by incorporating an EDFGL. (2) Generates a seed signal to the second stage and the power of this seed signal automatically varies according to the power of the total input signals.	(1) The seed signal compensates the power variations of the input signals. (2) Provides large gains for L-band signals.
Config 4-2	(1) Works as a pre-amplifier without clamping. (2) Works in the unsaturated regime due to short EDF length and small cross section parameters in L-band.	(1) Clamps the signal gains in the second stage by incorporating an EDFGL. (2) Works as a booster to provide high gains for L-band signals.

Table 4.1 Comparison of the functions of each stage for partially gain-clamped two-stage L-band EDFAs.

4.3. Simulation Model and Amplifier Parameters

4.3.1 Model

We simulate amplifier performance in the steady state (static case) using the two-level model described in Chapter 2. For simplicity, effects such as excited-state

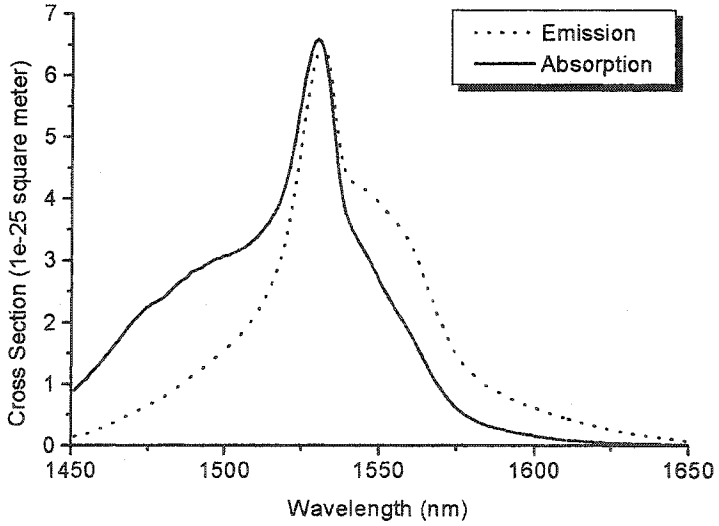

Fig. 4.2 EDF absorption (solid) and emission (dotted) cross-sections used in the numerical simulations.

absorption and inhomogeneous broadening are not considered. A commercial erbium-doped silica fiber (EDF741 Highwave Optical Technologies) is used in both simulations and experiments. The absorption and emission cross-sections are shown in Fig. 4.2 and the properties of the EDF are given in Table 4.2.

Parameter	Value
Lifetime	10ms
Overlap Factor	0.6 for signals at 1450-1650nm 0.8 for pump at 980nm
Numerical Aperture	0.25
Core Diameter (μm)	3
Erbium Diameter (μm)	2.8
Erbium Concentration (ppm)	≈ 500

Table 4.2 Parameters of EDF used in simulations and experiments

As before, the amplified spontaneous emission (ASE) noise is spectrally resolved from 1450-1650nm with 1nm resolution. We use a fourth-order Runge-Kutta method and an iteration routine to solve the more than 400 propagation equations.

4.3.2 Amplifier Parameters

We simulated and assembled the two EDFA configurations shown in Fig. 4.1. For both configurations, the EDF lengths are $L_1 = 20m$ and $L_2 = 100m$ (both stages use the same type of EDF); the pump wavelength is 980nm and the pump powers are 20mW and 90mW for stages 1 and 2, respectively (with co-propagating pump and signal in both stages). The FBGs used in our experiments are all centered at ≈ 1565nm with reflectivities $R_1 = 99\%$ and $R_2 = 95\%$ or 5%. Losses (from splices and insertion losses due to passive components such as isolators and couplers) are estimated to be ≈2dB for

both amplifier configurations (these losses are assumed to be wavelength independent when used in the simulations). Unless otherwise noted, we always use these parameters in our simulations and experiments.

4.4. Results

4.4.1 Results for Config 4-1

(1) Gain Clamping Performance

First, we evaluate the gain-clamping effect for Config 4-1. The feedback wavelength (i.e. FBG wavelength) is $\lambda_f = 1565nm$ and we set the signal wavelength to $\lambda_s = 1580nm$. Fig. 4.3 shows the simulated and measured gain as a function of input signal power for different feedback levels. The results show that the amplifier exhibits

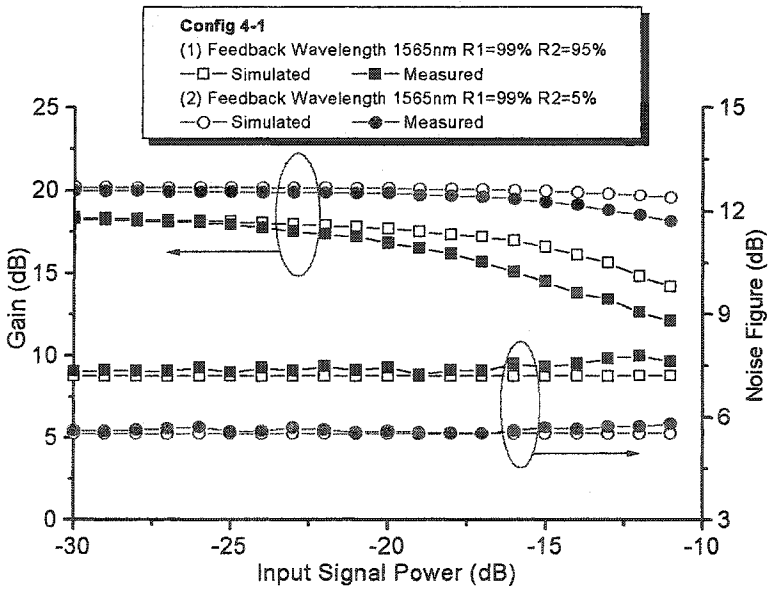

Fig. 4.3 Simulated and measured gain and NF as a function of input signal power for different feedback levels for Config 4-1. λ_s= 1580nm, L_1=20m, L_2=100m, P_1=20mW, P_2=90mW.

very good gain-clamped performance in the small signal regime both for $R_2 = 95\%$ and $R_2 = 5\%$. As can be seen, the amplifier shows higher gain $G = 20dB$ and larger $P_{crit} = -14dBm$ when $R_2 = 5\%$ compared to the case $R_2 = 95\%$ where $G = 18dB$ and $P_{crit} = -21dBm$. The difference in gain for two cases results from different feedback levels used in the first stage, which leads to a small change of the average N_2. The difference of P_{crit} is due to the fact that when R_2 is smaller, more power from the seed signal is input into the second stage, thereby compensating a larger variation in the total input signal power.

We also find that a lower NF is obtained when $R_2 = 5\%$ (<6dB compared to ≈7.5dB when $R_2 = 95\%$). For a two-stage EDFA with an isolator in the middle, the overall NF is mainly determined by that in the first stage. It has been shown that lower feedback level can lead to a better NF in a single-stage EDFA in Chapter 3. Therefore, the small R_2 results in a better NF of the overall amplifier. Note that there is very good agreement between our simulated and measured results and we attribute the slight differences to the non-ideal characteristics of the passive components (which may, for example, cause some loss of pump power to the various stages).

(2) Gain and NF Spectra

Next, we investigate the gain and NF spectra for different feedback wavelengths and feedback levels (i.e. different R_2). In Fig. 4.4, we show the simulated and measured gain and NF spectra for different feedback levels. As can be seen, for a fixed

$\lambda_f = 1565nm$, the gain and NF spectra can depend on the value of R_2. While the shape of the gain spectrum is approximately the same, a larger gain is obtained for smaller R_2. When $R_2 = 95\%$, the NF is quite high, especially in the region of 1570nm-1580nm, and a NF=9dB is measured at 1571nm. When we use the low reflectivity grating ($R_2 = 5\%$), a better NF spectrum is obtained and a maximum NF=6dB is measured over the 1570nm-1610nm range. Compared to the simulations, the experimental results show a slight degradation in NF for longer wavelengths ranging from 1595-1610nm. This is primarily due to the passive components which are optimized for 1550nm as well as the possibility of ground state and excited state absorption (which are not considered in the numerical model). Besides, the impact of ESA is not considered in the simulations, which may have some impact on longer wavelengths, especially for wavelengths beyond 1600nm.

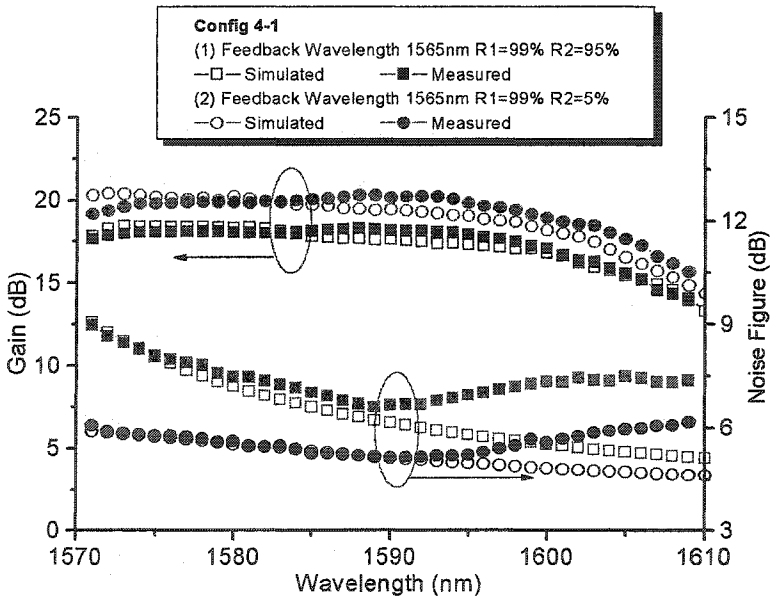

Fig. 4.4 Simulated and measured gain and NF spectra for different feedback levels for Config 4-1. Input signal power = -25dBm, L_1=20m, L_2=100m, P_1=20mW, P_2=90mW.

In Fig. 4.5, we show the impact of the feedback wavelength on the gain and NF spectra (using numerical simulations only). We use $R_1 = 99\%$ and $R_2 = 95\%$ to set the feedback level and consider two cases: $\lambda_f = 1560nm$ and $\lambda_f = 1565nm$. As can be seen, the flatness of the gain spectrum changes significantly with the feedback wavelength; on the other hand, the NF spectrum is relatively unaffected.

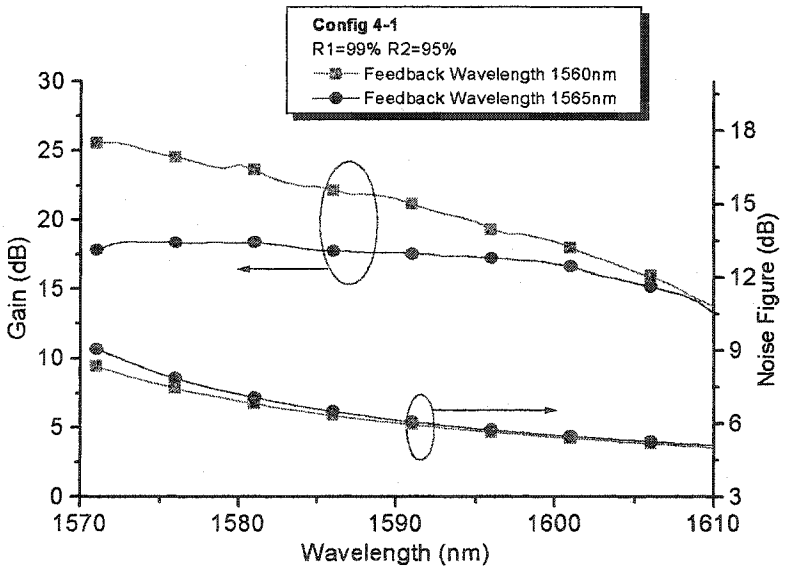

Fig. 4.5 Simulated gain and NF spectra for different feedback wavelengths for Config 4-1. Input signal power = -25 dBm, L_1=20m, L_2=100m, P_1=20mW, P_2=90mW.

4.4.2 Results for Config 4-2

As illustrated in Fig. 4.6, Config 4-2 also exhibits good gain-clamped characteristics. The critical powers are –13dBm and –17 dBm when R_2=95% and 5%, respectively. Moreover, a low noise figure is obtained for both feedback levels: NF=5dB for R_2=95% and NF=4dB for R_2=5%. In fact, the motivation for Config 4-2 is to achieve a better NF. In the section 4.1, we mentioned that the overall noise figure for a two-stage EDFA is mainly decided by that in the first stage. By simply moving the clamping stage to the second stage, there is no NF degradation in the first stage such that a very low overall NF can be achieved. The good noise performance for Config 4-2 can be seen further in Figs.4.7 and 4.8, which shows the NF spectrum (and gain spectrum) for different feedback levels and feedback wavelengths. (the simulations show that the

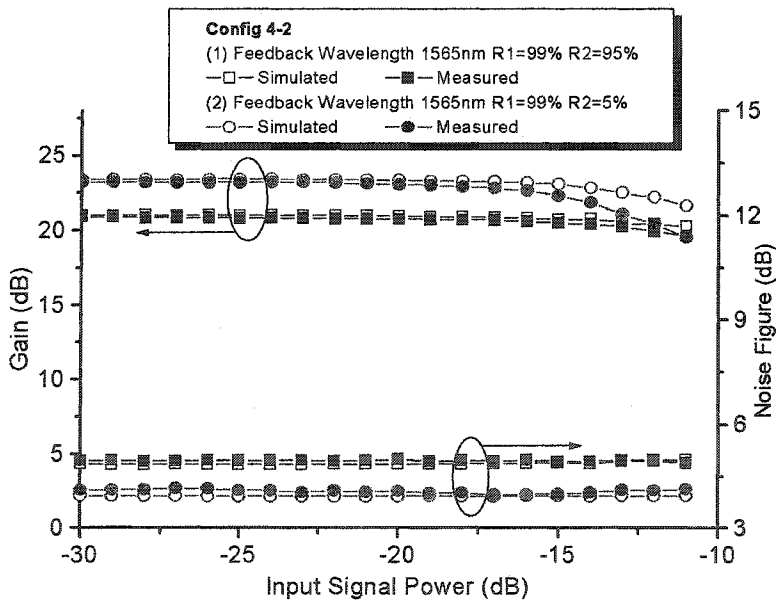

Fig. 4.6 Simulated and measured gain and NF as a function of input signal power for different feedback levels for Config 4-2. λ_s= 1580nm, λ_f =1565nm, L_1=20m, L_2=100m, P_1=20mW, P_2=90mW.

NF<5dB over the 1570nm-1610nm range for both R_2=95% and 5%). As before, the degradation in the measured NF at longer wavelengths arises primarily due to the wavelength dependence of the passive components. If these are designed for specific operation in the L-band, then the NF in the range of 1595-1610nm can be lowered further such that good noise performance can be obtained over the entire L-band (as predicted by simulations).

From Figs. 4.7 and 4.8, we see that changing the feedback level or feedback wavelength can alter the flatness of the gain spectrum and the amount of gain provided. For a given $\lambda_f = 1565nm$, a flatter gain spectrum can be obtained with R_2=95%, albeit at the expense of smaller gain and slightly higher NF compared with R_2=5%. On the other hand, for a given feedback level (R_1=99% and R_2=95%), $\lambda_f = 1565nm$ results in a flatter

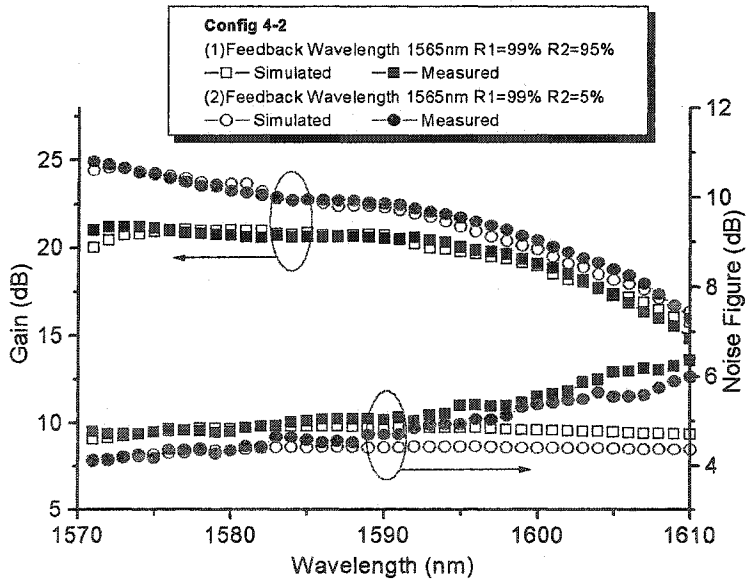

Fig. 4.7 Simulated and measured gain and NF spectra for different feedback levels for Config 4-2. Input signal power = -25dBm, L_1=20m, L_2=100m, P_1=20mW, P_2=90mW.

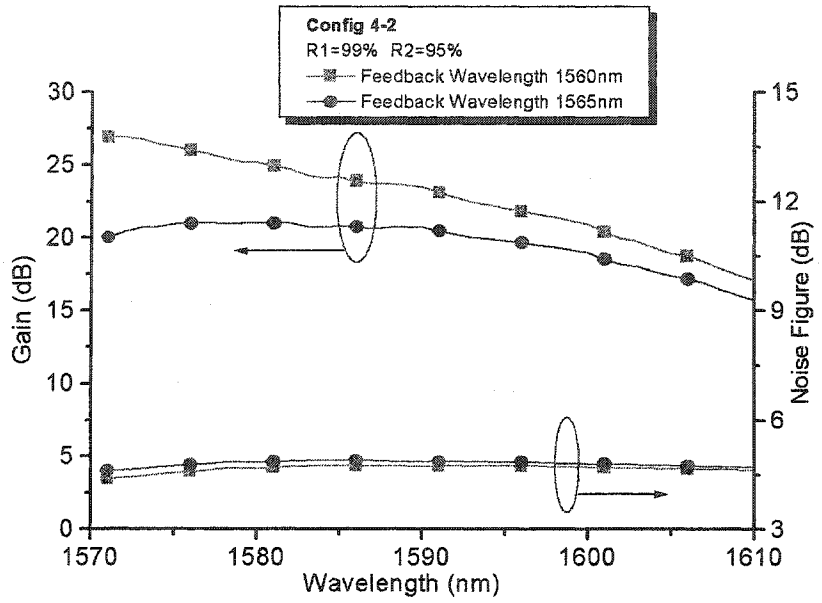

Fig. 4.8 Simulated gain and NF spectra for different feedback wavelengths for Config 4-2. Input signal power = -25dBm, L_1=20m, L_2=100m, P_1=20mW, P_2=90mW.

gain spectrum (with less gain) and insignificant change in NF spectrum compared with $\lambda_f = 1560nm$.

4.5. Discussion

4.5.1 Feedback Levels of R_1 and R_2

In single-stage gain-clamped EDFAs, we discussed that we can exchange the feedback levels of R_1 and R_2 without affecting the gain and NF. However, in Config 4-1, R_2 should be set to lower than R_1 since we need the EDFGL to generate a large seed signal for the second stage. For Config 4-2, R_1 and R_2 can be set asymmetrically or symmetrically according to the requirements without affecting the overall gain, P_{crit} and

flatness of gain spectrum, provided that the feedback level is the same. This can be seen in section 3.4.1 and Fig. 3.14 in Chapter 3.

4.5.2 Comparison of Config 4-1 and Config 4-2

(1) Gain, NF and P_{crit}

Comparisons for EDFA configurations are generally based on equal amplifier gain and noise figure (i.e. the pump power, EDF coil lengths, etc. are varied in order to achieve the same amplifier performance). However, for a gain-clamped amplifier, the critical power is also a very important performance metric in addition to the gain and NF. Since P_{crit} is a function of pump powers, it is hard to compare the critical power in two different configurations with different pump power. Therefore, we compare the gain-clamped amplifiers based on the following conditions: (a) the same coil length of EDF; (b) the same pump power; (c) the same feedback wavelength and feedback level.

(2) Comparison of Gain and P_{crit}

We first compare the two configurations by fixing the coil length of EDF and pump powers. We summarize the results obtained in section 4.4 for the two configurations, see Table 4.3. It is found that when the feedback level is high (95%), Config 4-2 shows a higher gain and a significantly larger P_{crit} than Config 4-1. But when the low feedback level (5%) is used, both configurations show large critical powers. This manifests that

Config 4-1 is only suitable for working at low feedback levels whereas Config 4-2 can have good performance at both high and low feedback levels.

		Config 4-1			Config 4-2		
Feedback Wavelength	Feedback Level	Gain	NF	P_{crit}	Gain	NF	P_{crit}
1560nm (simulation)	95%	24.1dB	6.9dB	-23dBm	25.2dB	4.7dB	-17dBm
1565nm (experiments)	95%	18.1dB	7.3dB	-21dBm	20.9dB	4.9dB	-13dBm
1565nm (experiments)	5%	20.1dB	5.6dB	-14dBm	23.2dB	4.0dB	-17dBm

Table 4.3 Comparisons of Config 4-1 and Config 4-2, $\lambda_s = 1580nm$

(3) Comparison of NF

It can be seen in Table 4.3 that Config 4-2 shows much lower NF than Config 4-1 in both high and low feedback levels and different feedback wavelengths. Since all parameters have NOT been optimized for either configuration, these results can be treated as a general comparison for both configurations.

On the other hand, in order to compare the noise performance of the two amplifiers more fairly, we optimize their design to provide the same small-signal gain and critical power, and to operate with the same input signal power conditions. To obtain a small-signal gain of 20.8dB (at λ_s=1580nm) and P_{crit}=-8dBm, the optimized designs are as follows: for Config 4-1, L_1=20m, L_2=100m, P_1=44mW, P_2=150mW, R_1=99%, and R_2=50%; for Config 4-2, L_1=10m, L_2=100m, P_1=30mW, P_2=100mW, R_1=99%, and R_2=95%. In Fig. 4.9, we show the simulated gain as a function of input signal power.

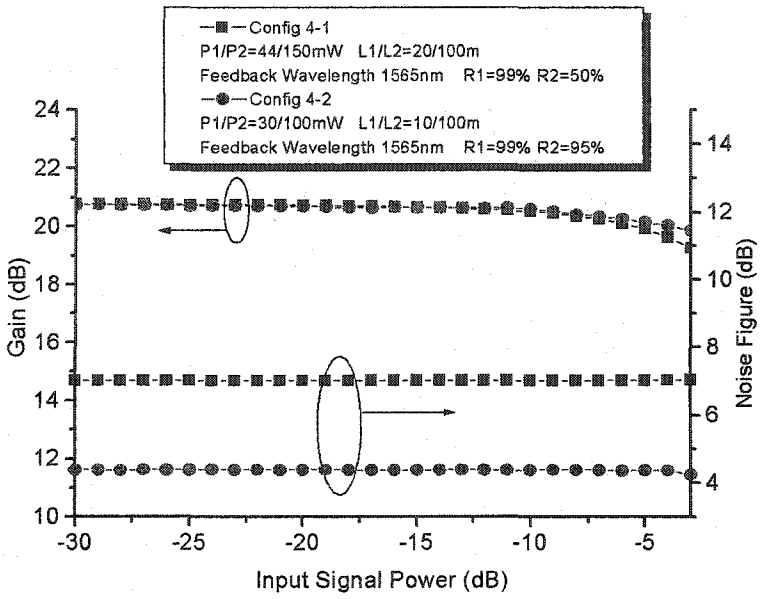

Fig. 4.9 Simulated gain and NF as a function of input signal power for both configurations when the amplifiers are optimized to provide a gain of 20.8dB and P_{crit} =-8dBm. λ_s= 1580nm, input signal power = -25dBm.

Both amplifiers provide the required gain and critical power. However, Config 4-2 requires 10m less EDF and 64mW less total pump power. More importantly, the noise performance is quite different and in particular, Config 4-2 has a NF≈4dB whereas Config 4-1 has a NF≈7dB. When we attempted to design Config 4-1 to provide not only the same gain and critical power but also the same NF (4dB) as Config 4-2, we found that, in addition to changing P_1 and P_2, we required R_2<0.1% which may be difficult to realize practically. On the other hand, it is straightforward to achieve the grating reflectivities to obtain the low noise performance for Config 4-2. Finally, we note that changing the pump power for both stages (in either configuration) can change the critical power without affecting the NF.

4.6 Conclusion

We have investigated two configurations of two-stage L-band EDFAs with gain-clamped characteristics, both of which use partial gain-clamping (only one of the two stages is truly gain-clamped). FBGs have been used in both configurations to form an EDFGL that clamps the gain of one stage. Although the two configurations have a very simple physical difference, their underlying principles of operation are considerably different which, in turn, causes differences in performance. Both designs can exhibit good overall gain-clamped characteristics and Config 4-2 (in which the second stage is gain-clamped) can obtain a NF as low as 4dB. This has been observed both theoretically and experimentally. When both amplifiers are optimized to provide the same gain and critical power (for a given signal wavelength), Config 4-2 requires a shorter length of EDF and less total pump power. Furthermore, a low NF can be readily obtained. These results show that a partially gain-clamped two-stage amplifier, in which the second stage is gain-clamped by an EDFGL, can potentially be used for efficient gain control for L-band EDFAs.

References

[4.1] B. Pedersen, M. L. Dakss, and W.J. Miniscalco, "Conversion efficiency and noise in erbium-doped fiber power amplifiers," *Optical Fiber Amplifiers and Their Applications*, vol. 13, pp. 170-176, 1991.

[4.2] Richard I. Laming, Michael N. Zervas, and David N. Payne, "Erbium-Doped Fiber Amplifier with 54 dB Gain and 3.1 dB Noise Figure," *IEEE Photonics Tech. Lett.,* vol. 4, no. 12, pp.1345-1347, 1992.

[4.3] S. Yamashita and T. Okoshi, "Performance Improvement and Optimization of Fiber Amplifier with a Midway Isolator," *IEEE Photon. Tech. Lett.,* vol. 4, no.11, pp.1276-1278, 1992.

[4.4] K. Inoue, "Gain-clamped fiber amplifier with a short length of preamplification fiber," *IEEE Photon. Technol. Lett.,* vol. 11, no. 9, pp. 1108-1110, 1999.

[4.5] M. A. Mahdi and H. Ahmad, "Long-wavelength-band Er3+-doped fiber amplifier incorporating a ring-laser as a seed signal generator," *IEEE J. Sel. Topics in Quantum Electron.,* vol. 7, no. 1, pp. 59-63, 2001.

Chapter 5 Dynamic Properties of Gain-Clamped EDFAs

5.1 Introduction

In Chapters 3 and 4, we discussed the static properties of all-optical gain-clamped EDFAs. In this chapter, we focus on their dynamic properties.

We have shown that all-optical gain-clamped EDFAs can provide stable gain in the steady state when the total input power varies within the dynamic range due to the channel add/drop operations. However, dynamic gain (power) excursion and transient time are still serious problems for these amplifiers. It is well known that EDFAs have very slow gain dynamics due to the long lifetime of erbium ions. The typical recovery times (i.e. time to reach the steady state) are in the range of $100\mu s$ to 1ms for C-band and as long as 10ms for L-band operation. During the transient time, the gain of the surviving signals can be higher (overshoot) or lower (undershoot) than that in the steady state, thereby causing transient errors at the receiver. Moreover, for a long-haul transmission system with cascaded EDFAs, the gain excursion problem becomes more serious since the gain variation of each amplifier will accumulate along the fiber link [5.1].

A number of methods have been demonstrated to control the undesired gain excursions of the surviving channels in EDFAs, which include pump control [5.2] and all-optical gain control with ring feedback laser structures [5.3] or with FBG laser structures [5.4]. Although it has been demonstrated that all-optical gain-clamping can reduce the gain excursion, it can suffer from relaxation oscillations and spectral-hole burning (SHB) effects which cause power over/under –shoot with fast oscillations and residual variations in signal gain (in turn this degrades the system performance of the

surviving channels) [5.5-5.6]. However, these investigations are all based on all-optical gain control with ring feedback laser structures with large cavity losses and no research has been done on FBG configurations, in which a high feedback level can be applied.

We theoretically and experimentally investigate the gain dynamics of the two configurations of two-stage L-band EDFAs with partial gain-clamping that we proposed in Chapter 4 (Config 4-1 and Config 4-2). In the following sections, we show both experimental results and simulation analysis. In the simulations, we do not include some inhomogeneous effects such as spectral hole burning in our model since the inhomogeneous model of an EDFA is very complicated and we do not know the exact broadening of the erbium ions. Thus we only obtain qualitative agreement between experiment and simulation results.

5.2 Experiments

5.2.1 Experimental Setup

The experiment setup is shown in Fig. 5.1. The parameters for the amplifiers are as follows: $L_1 = 20m$, $L_2 = 100m$, $P_1 = 20mW$, $P_2 = 90mW$, $R_1 = 99\%$, $R_2 = 95\%$. The exactly same coils of EDF that are used for steady-state experiments described in Chapter 4 are chosen. We choose $\lambda_s = 1585nm$ as the surviving channel and another signal at 1590nm which is modulated at 100Hz to simulate the operation of channel add/drop. A 3dB coupler is used to multiplex the two signals. A FBG at 1585nm and a circulator form a wavelength selector to isolate the surviving channel at the output. We use a 25GHz

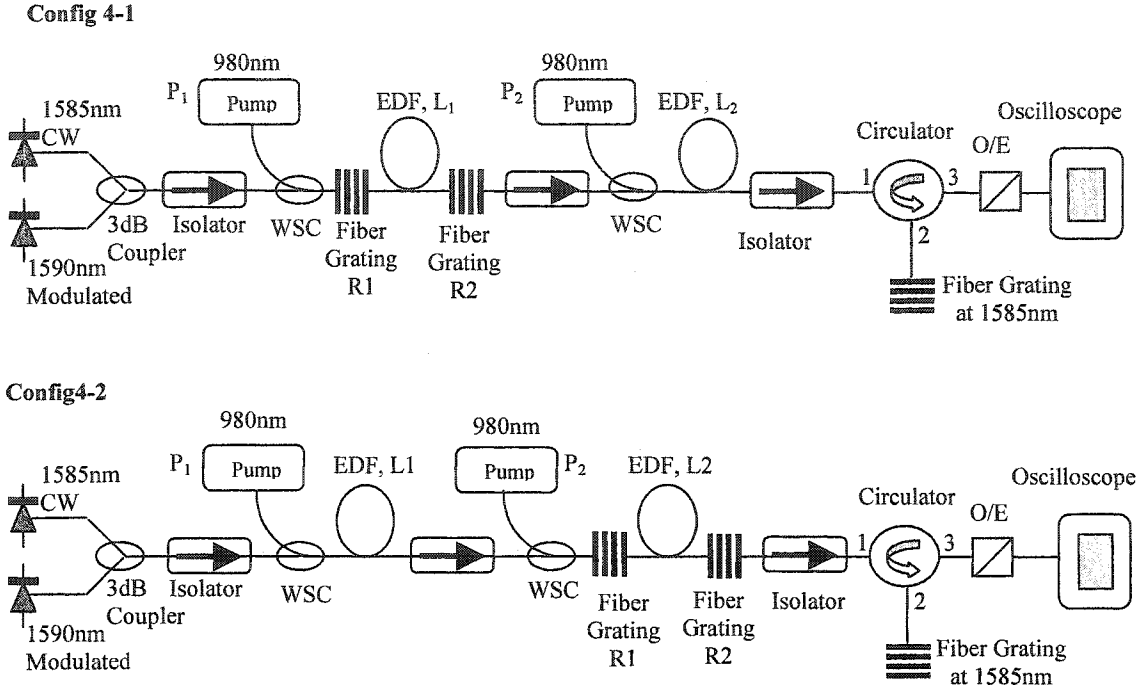

Fig. 5.1 Experiments setup for gain dynamics of two configurations of two-stage L-band EDFAs using partial clamping. $\lambda_s = 1585nm$, $L_1 = 20m$, $L_2 = 100m$, $P_1 = 20mW$, $P_2 = 90mW$, $R_1 = 99\%$, $R_2 = 95\%$.

high-speed photoreceiver from *NewFocus Inc.*, which is fast enough to detect any relaxation oscillations of the EDFAs in transients.

The input signal powers for the surviving channel and the add/drop channel are very important for the overall performance of the gain dynamics we obtain. If the total input signal power is in the small signal regime, the lasing signal power in the cavity can be very large compared to power changes in the signals, thereby suppressing the relaxation oscillations of the surviving channel. Therefore, we use the following rules to choose the powers of the surviving and modulated signals: (i) the total input signal power is kept equal to P_{crit} for both configurations to ensure gain-clamping; (ii) the power for

the surviving signal is fixed at –25dBm (the signal power is measured at the point that is between the 3dB coupler and the isolator at the input).

5.2.2 Result and Discussion

Fig. 5.2 shows the dynamic response of two configurations. When the total input power (surviving signal at 1585nm+modulated signal at 1590nm) is set equal to P_{crit}, the transient gains are shown in Fig.5.2 (a) and (c) for Config 4-1 and Config 4-2, respectively. Power excursions are observed in both cases and both configurations show small gain excursion (0.31dB for Config 4-1 and 0.29dB for Config 4-2). When we increase the total input power to 3dB higher than the critical power by simply increasing the power of the modulated signal (without changing the power of the surviving signal), the power excursions become 1.7dB and 0.71dB for Config 4-1 and Config 4-2,

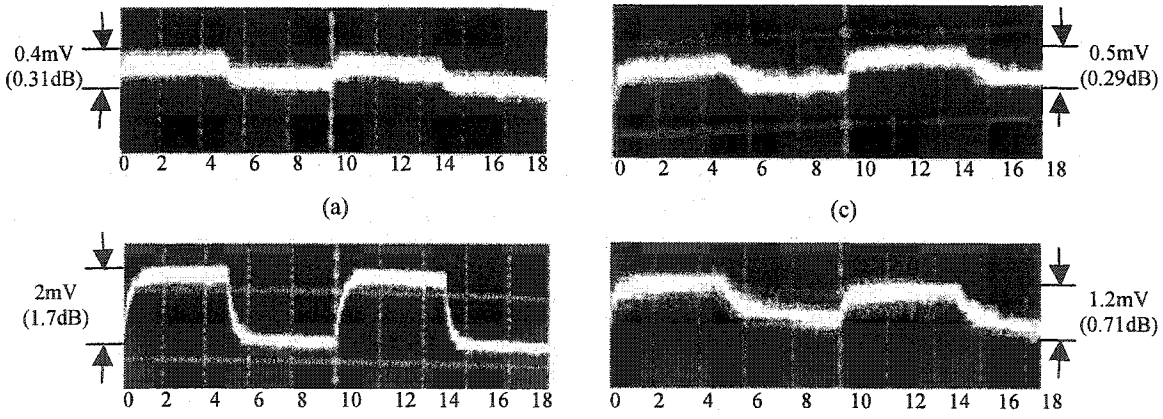

Fig. 5.2 Transient power excursion of the surviving channel at 1585nm for Config 4-1 where
(a) total input signal power is equal to the critical power (P_{total}= -21dBm, $P_{surviving}$= -25dBm),
(b) total input signal power is ≈3dB higher than the critical power (P_{total}= -18dBm, $P_{surviving}$= -25dBm), for Config 4-2 where
(c) total input signal power is equal to the critical power (P_{total}= -13dBm, $P_{surviving}$= -25dBm),
(d) total input signal power is 3dB higher than the critical power (P_{total}= -10dBm, $P_{surviving}$= -25dBm).

respectively, see Figs. 5.2(b) and (d). Therefore, it can be concluded that both configurations show good gain dynamics properties when the total power is set less or equal to P_{crit}.

The gain (power) excursions are mainly from three sources: (1) relaxation oscillation of the lasing signal; (2) inhomogeneous effects, such as spectral hole burning; and (3) partially gain-clamped structures. Our experimental results are the combination of these three factors.

Relaxation oscillations in Fig. 5.2 are not clearly seen. This is partly because we use a high feedback level in both cases ($R_1 = 99\%$ and $R_2 = 95\%$). Richards et al. [5.7] theoretically showed that the feedback level is an important parameter that affects the transient power excursions in the surviving channel and a high feedback level leads to small relaxation oscillations (note that a ring laser structure is used in their simulations). The explanations are as follows: in a gain-clamped EDFA, a high feedback level results in a very large lasing power inside the cavity. When channels are added/dropped, the signal power change is small compared to lasing power. Strong feedback from FBGs will greatly decrease the time for the lasing to rebuild, which suppresses the over/under shoot of the surviving channel. Therefore, relaxation oscillations are not the main contributor for power excursion. Furthermore, we showed in Chapter 4 that the partially gain-clamped structures we proposed can have good gain-clamping performance. Hence, we expect that SHB effect is the main cause for the power excursion since the separation between λ_f and λ_s is quite large ($\approx 20\,\text{nm}$).

5.3 Modeling and Simulation

5.3.1 The Dynamic Model

The dynamic model uses both space and time dependent (z and t) rate equations (2.16) and propagation equations (2.14-2.15). Therefore, solving a set of partial differential equations is key in the simulations. The method we used is to decompose the space and time into a grid of $M \times N$ discrete bins Δz and Δt, respectively. First, we calculate the equation in the steady state and record the field powers $P_k(z,t=0)$ and upper state population $N_2(z,t=0)$ at each grid point of the space domain. The ASE noise spectra are resolved from 1450nm-1650nm with 1nm resolution. These values are used as the initial condition to calculate the upper state population for the first step. And then we can integrate the space equations by these values of $N_2(z,\ t=1\cdot\Delta t)$ to calculate the field powers of signals, ASE noise spectrum and so on in the space domain. These values are used to calculate the upper state population at the next time step $2\Delta t$ and we can obtain all field powers at $t=2\Delta t$. By this iteration routine, we can accurately characterize the dynamic behaviors of EDFAs.

In the dynamic model, the time step Δt is critical in capturing the dynamic behavior of the EDFAs. A small Δt results in good accuracy but requires a long calculation time while a large Δt enlarges simulation errors. It has been shown that Δt should be less than t_{cavity} (the cavity round trip time) in order to keep the accuracy for modeling a C-band gain-clamped EDFA [5.2]. In our L-band model, we choose

$\Delta t = 10ns$ where the speed of light in EDF is assumed to be 5ns/meter (we assume $n=1.5$ and n/c=5ns/m).

5.3.2 Configuration

We simulate the dynamic response of the two configurations as shown in Fig 5.1 (Config 4-1 and Config 4-2). All parameters for the amplifiers are exactly the same as those used in the experiments, such as length of EDF and pump power. We still use signals at 1585nm and at 1590nm to simulate the surviving channel and add/drop channels, respectively. The modulation rate we used in the simulations is 100Hz.

Since the dynamic model we used here assumes a completely homogeneous medium, all simulation results do not include any inhomogeneous effects. Therefore, there will be no SHB effects on the signal gain although λ_s and λ_f are separated by 20nm. The gain excursion is mainly from relaxation oscillations and the partially gain-clamped amplifier structures. Therefore, we cannot quantitatively compare the simulation and experimental results. However, our dynamic model can be used as a reference for the experiments.

5.3.3 Simulation Results

Fig. 5.3 and Fig. 5.4 show the transient gain excursions of the surviving channel at 1585nm for both Config 4-1 and Config 4-2. First of all, it can be seen that there are no relaxation oscillations in both cases. This confirms the conclusion made by Richards et al. [5.7] that a high feedback level results in small relaxation oscillations. On the other

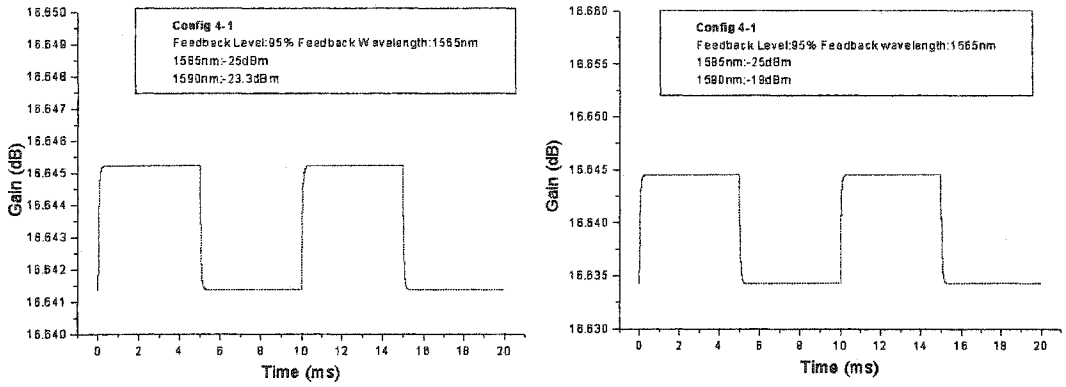

(a) (b)

Fig. 5.3 Simulation results of transient gain excursion of the surviving channel at 1585nm for Config 4-1, λ_s= 1585nm, λ_f=1565nm, L_1=20m, L_2=100m, P_1=20mW, P_2=90mW.
(a) total input signal power is equal to the critical power (P_{total}= -21dBm, $P_{surviving}$= -25dBm);
(b) total input signal power is ≈3dB higher than the critical power (P_{total}= -18dBm, $P_{surviving}$= -25dBm)

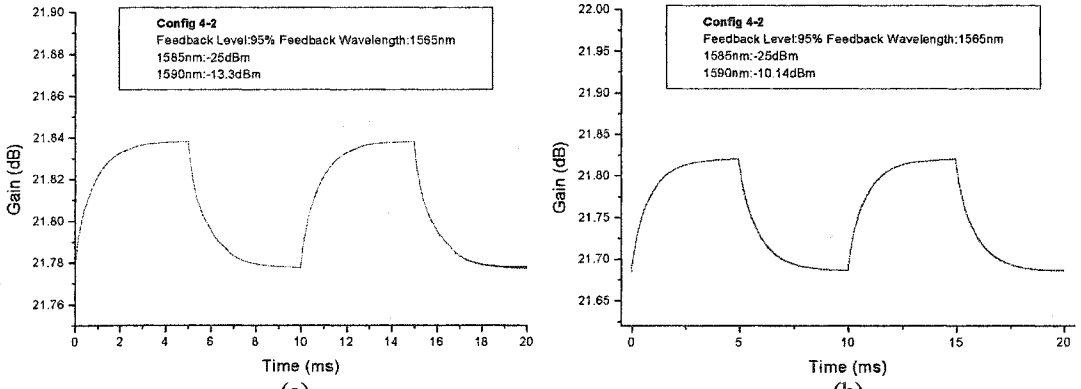

(a) (b)

Fig. 5.4 Simulation results of transient gain excursion of the surviving channel at 1585nm for Config 4-2, λ_s= 1585nm, λ_f=1565nm, L_1=20m, L_2=100m, P_1=20mW, P_2=90mW.
(a) total input signal power is equal to the critical power (P_{total}= -13dBm, $P_{surviving}$= -25dBm);
(b) total input signal power is ≈3dB higher than the critical power (P_{total}= -10dBm, $P_{surviving}$= -25dBm)

hand, both configurations show very small gain excursions (0.003dB for Config 4-1 and 0.06dB for Config 4-2 when P_{total} is equal to P_{crit}). When we increase the P_{total} to 3dB higher than P_{crit}, the gain excursions become larger (0.01dB for Config 4-1 and 0.15dB for Config 4-2). Since inhomogeneous effects such as SHB are not included in the simulations, these gain excursions have two contributions; one is relaxation oscillation of

the surviving channel; the second is derived by partially gain-clamped structures, in which only one stage is truly clamped. Since there are no relaxation oscillations observed, we deduce that all gain excursions are from the partially gain-clamped amplifier structures.

From Fig. 5.3 and Fig. 5.4, it can be seen that gain excursions of Config 4-2 is larger than that of Config 4-1, which is different from our experimental results as shown in Fig 5.2. This is because we do not include inhomogeneous effects such as SHB in our simulations, which can have a large impact on the gain excursions of the amplifiers. Furthermore, we use different total input signal powers for the two amplifier structures due to their different critical powers ($P_{total} = -21dBm$ for Config 4-1 and $P_{total} = -13dBm$ for Config 4-2). Therefore, Config 4-1 may suffer more inhomogeneous gain from SHB than Config 4-2 because of its smaller input signal power.

Although these results cannot be used to compare with experimental results in values, they show the same trends of what we obtained in experiments; i.e. small gain excursion and no relaxation oscillations. Small gain excursions in both configurations also manifest that partially gain-clamped structures can effectively clamp the signal gain in both static and dynamic states.

The suppression of relaxation oscillations in our gain-clamped amplifiers come from the high feedback level used in the system. In order to prove this, we simulate transient gain excursions of Config 4-2 at a lower feedback level ($R_1 = 99\%$ and $R_2 = 10\%$) as shown in Fig. 5.5, with $P_{total} = -17dBm$, $P_{surviving} = -25dBm$ (all other amplifier parameters are the same as before). In order to observe the relaxation

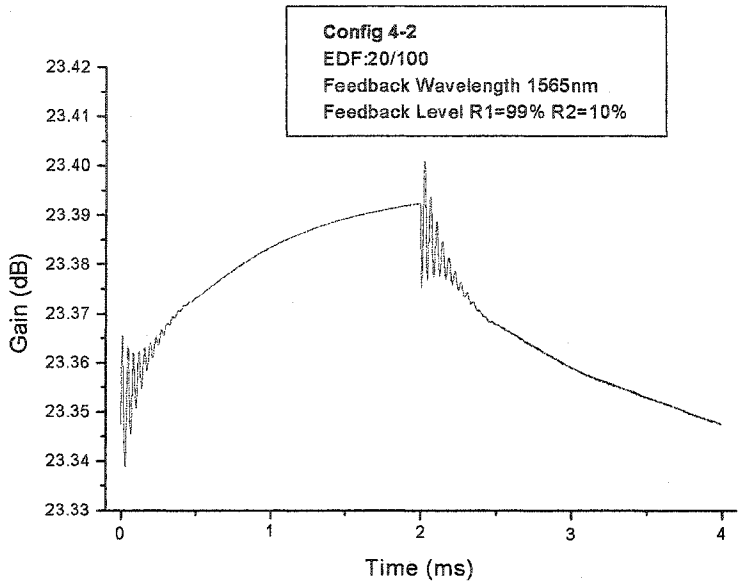

Fig. 5.5 Simulation results of transient gain excursion of the surviving channel at 1585nm for Config 4-2. The total input signal power is equal to the critical power (P_{total}= -17dBm, $P_{surviving}$= -25dBm),

oscillations clearly, we change the modulation rate to 250Hz. As shown in Fig. 5.5, oscillations of the surviving channel at 1585nm are quite large. When the feedback level becomes lower, relaxation oscillations can have a larger impact on transient gain excursions.

5.4 Conclusion

We have presented experimental and theoretical analyses of the dynamic properties for two-stage L-band EDFAs with partial gain-clamping. First, we experimentally investigate the gain dynamics for both configurations and our results show that small gain (power) excursions are found for both cases and almost no relaxation oscillations are observed. Second, we simulate the transient response with a dynamic homogenous model, which excludes all inhomogeneous effects such as SHB. We find that the amount of relaxation

oscillations depend on the feedback level: with a high feedback level, there are almost no relaxation oscillations while when a low feedback level is applied, large relaxation oscillations are observed.

References

[5.1] S. Y. Kim, J. Chung, and B. Lee, "Dynamic performance of the all-optical gain-controlled EDFA cascade in multiwavelength optical networks," *Electron. Lett.*, vol. 33, no. 14, pp. 1475-1477, 1997.

[5.2] A. K. Srivastava, Y. Sun, J.L. Zyskind, J.W. Sulhoff, C. Woff, and R.W. Tkach, "Fast gain control in erbium-doped fiber amplifier," *in Optical Amplifier and Their Applications*, vol. 5, 1996.

[5.3] G. Luo, J. L. Zyskind, Y. Sun, A. K. Srivastava, J. W. Sulhoff, C. Wolf, and M. A. Ali, "Performance degradation of all-optical gain-clamped EDFAs due to relaxation oscillations and spectral-hole burning in amplified WDM networks," *IEEE Photon. Technol. Lett.*, vol. 9, pp. 1346-1348, 1997.

[5.4] J. F. Massicott, S. D. Willson, R. Wyatt, J.R. Armitage, R. Kashyap, D. Willams, and R. A. Lobbett, "1480nm pumped erbium doped fiber amplifier with all optical gain control." *Electron. Lett.*, vol. 30, pp.962-964,1994.

[5.5] S.-J. Sheih, J. W. Sulhoff, K. Kantor, Y. Sun, and A. K. Srivastava, "Dynamic behaviour in L-band EDFA," *Proc. Conf. on Opt. Fiber Commun.*, vol. 2, pp. 125-127 2000.

[5.6] D. Gurkan, M. I. Hayee, and A. E. Willner, "Transient behaviour of L-band and C-band EDFAs in an add/drop multiplexed 40-channel WDM network," *Proc. Conf. on Lasers and Electro-Optics*, pp. 415-416, 2001.

[5.7] D. H. Richards, J. L. Jackel, and M. A. Ali, "A theoretical investigation of dynamic all-optical automatic gain control in multichannel EDFA's and EDFA cascades," *IEEE J. Sel. Topics in Quantum Electron.*, vol. 3, no. 4, pp. 1027-1036, 1997.

Chapter 6 Conclusion

In this thesis, we have presented systematic studies of all-optical gain-clamped L-band EDFAs using simulations and experiments. Single-stage and two-stage EDFA structures with different gain-clamping mechanisms are investigated, while experiments of two-stage L-band EDFAs with partially gain-clamped amplifier structures have been measured in order to evaluate the simulation results.

We explored single-stage gain-clamped L-band EDFAs. We compared two gain-clamping configurations: a ring feedback configuration (Config 3-1) and a FBG configuration (Config 3-2). The results show that both structures have good and similar gain-clamping effects at low feedback level. However, Config 3-1 suffers large gain loss at a high feedback level while Config 3-2 can be applied to any feedback level.

Based on the single-stage gain-clamped EDFA structures, we investigated two configurations (Config 4-1 and Config 4-2) of two-stage L-band EDFAs with partial gain-clamping (only one of the two stage is truly gain-clamped), in which a pair of FBGs have been used to form an EDFGL that clamps the gain of one stage. Although the two configurations have a very simple physical difference, their underlying principles of operation are considerably different which, in turn, causes differences in performance. Both designs can exhibit good overall gain-clamped characteristics and Config 4-2 (in which the second stage is gain-clamped) can obtain a NF as low as 4dB. This has been observed both theoretically and experimentally. When both amplifiers are optimized to provide the same gain and critical power (for a given signal wavelength), Config 4-2

requires a shorter length of EDF and less total pump power. Furthermore, a low NF can be readily obtained.

We also explored the dynamic performances for Config 4-1 and Config 4-2. We experimentally find that when the total input signal powers to Config 4-1 and Config 4-2 are equal to the critical power, the gain excursions are 0.31dB and 0.29dB, respectively. When we increase the input signal power to 3dB higher than the critical power, the gain excursions are 1.7dB and 0.71dB, respectively. Since these results are experimentally obtained which are the combination effects of 3 contributors: relaxation oscillations, spectral hole burning and the fact that the amplifiers are only partially gain-clamped.

We also simulate the gain dynamics using a homogeneous model, in which SHB is excluded. The gain excursions are 0.003dB and 0.06dB for Config 4-1 and Config 4-2 when the total input signal powers are equal to the critical power. When the total signal powers are 3dB higher than the critical power, the gain excursions for Config 4-1 and Config 4-2 are 0.01dB and 0.15dB, respectively. It is clear that the relaxation oscillations in both configurations are very small, which mainly results from using the higher feedback level (around 95%) in the clamping stage. When a low feedback level (around 10%) is applied in our simulations, relaxation oscillations become obvious and have a large impact on the transient response. Hence, our simulation results agree with experimental results that relaxation oscillations can be removed by using high feedback level in both all-optical partially gain-clamped EDFA structures. In our simulations, Config 4-1 shows smaller gain excursions than Config 4-2. This is because we do not include inhomogeneous effects in our simulation, which can have very different impact

on two configurations when the total input signal powers for the two amplifier structures are different. In the future, we will develop an inhomogeneous EDFA model to quantify how inhomogeneous effects can impact the transient responses of EDFAs.